T.R.
BOLU ABANT İZZET BAYSAL UNIVERSITY
INSTITUTE OF GRADUATE STUDIES
Department of Physics

STRUCTURAL AND PHYSICAL PROPERTIES OF PRASEODYMIUM BASED MANGANITE SYSTEMS

MASTER IN SCIENCE

NOOR HADI AITRABI

ACADEMIC SUPERVISOR
Prof. Dr. Cabir Terzioğlu

BOLU, TEMMUZ - 2022

APPROVAL OF THE THESIS

structural and physical properties of praseodymium based manganite systems submitted by **Noor Hadi Altrabi** and defended before the Examining Committe Members listed below in partial fulfillment of the requirements for the degree of **Master of Science** in **Department of Physics, Institute of Graduate Studies of Bolu Abant Izzet Baysal University in 26.07.2022** by

Examining Committee Members	**Signature**
Supervisor Prof. Dr. Cabir Terzioğlu Bolu Abant Izzet Baysal University	.....
Member Prf. Dr. Muharrem Gökçen Duzce University	.....
Member Assoc.Prof. Dr .Sevgi Polat Altintas Bolu Abant Izzet Baysal University	.....

Prof. Dr. İbrahim KÜRTÜL

Director of Instıtute of Graduate Studies

ETHICAL DECLARATION

In this thesis dissertation that was properly prepared according to the Thesis Writing Rules of Bolu Abant İzzet Baysal University of the Institute of Graduates Studies, I hereby declare that;

- All data, information, and documents presented in the thesis were obtained in accordance with the academic and ethical rules,
- All data, documents, assessments, and results were presented in accordance with the scientific ethical and moral rules,
- All works that were benefitted in the thesis were appropriately cited,
- No alteration was made in the data used,
- Study presented in this thesis is original,

Otherwise, I declare that I accept the loss of all my rights in case any contradiction that may arise against me.

Based on the plagiarism report that was generated on the date of 2022/5/15 by using predetermined filtrations set by Directorate of Institute of Graduate Studies of the Turnitin programme, a plagiarism detection sofware, the similarity index detected was 21 %.

_____

NOOR HADI HAMZAH AITRABI

ABSTRACT

STRUCTURAL AND PHYSICAL PROPERTIES OF PRASEODYMIUM BASED MANGANITE SYSTEMS
MSC THESIS
NOOR HADI ALTRABI
BOLU ABANT IZZET BAYSAL UNIVERSITY
INSTITUTE OF GRADUATE STUDIES
DEPARTMENT OF PHYSICS
(SUPERVISOR: PROF. DR. CABIR TERZIOĞLU)
BOLU, JULY 2022
(XII+ 40)

The structural and physical properties of Sr-doping in manganite perovskite oxides with the formula $Pr_{1-x}Sr_xMnO_3Fy$ (x = 0.2, 0.3, 0.4 and 0.5) were investigated in this study.

The samples were fabricated by the utilization of the solid-state reaction technique and were investigated by using X-ray diffraction, scanning electron microscope, and resistivity measurements as a function of temperature at constant dc magnetic fields. From x-ray powder diffraction measurements, all ceramics showed orthorhombic structure with space group N: 62 phases, and a second phase with space group N:141 appeared with sample Pr0.5Sr0.5MnO3. The investigation of the scanning electron microscope (SEM) revealed that as the Pr content of samples decreases the grain size of the samples decreases. The resistivity was measured for all samples under 0 T and 1 T dc magnetic field as a function of temperature. From these measurements, the insulator-metal transition temperature was obtained from the inflection point of (dp/dt) plots, and it was found that T MI shifted to higher temperatures as Sr content increased as noted in Pr0.5Sr0.5MnO3 the TMI = 315 K.

The magnetoresistance was found at about 39% for the sample with x = 0.3 with decreasing the praseodymium concentration lower MR% values were observed. The results obtained in this study show that the Pr-based manganites are promising materials to be used in temperature sensing devices.

KEYWORDS: Sr-doping, Magnetoresistance, Phase transition, T_{MI}

ÖZET

PRASEODMİYUM TEMELLİ MANGANİT SİSTEMLERİN YAPISAL VE FİZİKSEL ÖZELLİKLERİ
YÜKSEK LİSANS TEZİ
NOOR HADI ALTRABI
BOLU ABANT İZZET BAYSAL ÜNİVERSİTESİ
LİSANSÜSTÜ EĞİTİM ENSTİTÜSÜ
FİZİK ANABİLİM DALI
(TEZ DANIŞMANI: PROF. DR. CABİR TERZİOĞLU)
BOLU, TEMMUZ - 2022
(XII + 40)

Bu çalışmada manganit perovskit oksitlerde $Pr_{1-x}Sr_xMnO_3Fy$ (x = 0.2, 0.3, 0.4 ve 0.5) formülüne sahip Sr-katkılamanın yapısal ve fiziksel özellikleri incelenmiştir. Tüm malzemeler, katı hal reaksiyon tekniği kullanılarak üretilmiştir ve x-ışını kırınımı (XRD), taramalı elektron mikroskobu (SEM) ve sabit dc manyetik alanlarda sıcaklığın bir fonksiyonu olarak özdirenç ölçümleri ile araştırılmıştır. X-ışını toz kırınım ölçüm sonuçlarına göre tüm numuneler, N:62 uzay grubu fazı ile ortorombik yapı göstermiştir. Ayrıca, $Pr_{0.5}Sr_{0.5}MnO_3$ örneğinde N:141 uzay grubuna ait ikinci bir faz ortaya çıkmıştır. SEM sonuçlarına göre örneklerde Pr içeriği azaldıkça tane boyutlarının da azaldığı tespit edilmiştir. Çalışmada özdirenç, sıcaklığın bir fonksiyonu olarak 0 T ve 1 T dc manyetik alan altındaki tüm numuneler için ayrı ayrı ölçülmüştür. Elde edilen ölçüm sonuçlarına göre, (dp/dt) eğrilerinin büküm noktasından yalıtkan- metal geçiş sıcaklığı saptanmış ve Sr içeriği arttıkça TMI'nin daha yüksek sıcaklıklara kaydığı, $Pr_{0.5}Sr_{0.5}MnO_3$ T_{MI}=315 K, bulunmuştur.

$Pr_{0.5}Sr_{0.5}MnO_3$ ve T_{MI}=315 K'de belirtildiği gibi Sr içeriği arttıkça TMI'nin daha yüksek sıcaklıklara kaydığı bulunmuştur. Bu çalışmanın sonuçları ile Bu çalışmada elde edilen sonuçlar, Pr temelli manganitlerin sıcaklık algılama cihazlarında kullanılmak üzere oldukça umut verici malzemeler olduğunu göstermektedir.

ANAHTAR KELİMELER: Sr-doping , Manyetodirenç, Faz geçişi, T_{MI}

TABLE OF CONTENTS

LIST OF FIGURES

Page

LIST OF TABLES

Page

LIST OF PICTURES

Page

LIST OF ABBREVIATIONS AND SYMBOLS

MR : Magnetoresistance

AMR : Anisotropic Magnetoresistance

CMR : Colossal Magnetoresistance

DE : Double Exchange

EDAX : Energy Dispersive Analysis of X-Ray

GMR : Giant Magnetoresistance

K : Kelvin

OMR : Ordinary Magnetoresistance

SEM : Scanning Electron Microscope

TCR : Temperature Coefficient of Resistance

$\mathbf{T_{MI}}$: Metal-insulator transition temperature

T : Tesla

XRD : X-Ray Diffraction

t : Tolerance factor

ACKNOWLEDGEMENTS

I would like to express my deep gratitude and thanks to my supervisor Prof. Dr. Cabir Terzioğlu for his guidance and advice to complete this thesis , and Assos. Prof. Dr. Sevgi Polat Altıntaş for her advice, criticism, encouragement, and insight throughout the research. And for Dr. Nevin Soylu Koç for sharing with me her lab experience and her help to complete the measurements and Fatih Sabah who shared his knowledge with me.

I would also like to thank my mother and my family and friends who have supported me through this stage of my life

1. INTRODUCTION

For numerous optoelectronic and photonic device applications, Perovskite materials are known as the most attractive and effective low-cost energy sources, Because of the ability to include an extensive range of cations of different ionic sizes in ABO_3 crystal structure and the oxidation states of the A and B sites, which is the origin of a large variety of perovskites with a wide range of physical properties (1,2)

Because of that, these compounds have become the attention of many Studies that examine their ability among these materials is manganite perovskite, which has various and significant structural, magnetic and electrical properties.

Jonker and Santen discovered the magnetic characteristics of perovskite in 1950. One of the foundations on which the magnetic actions of these materials depends is the strength of interactions between Mn^{+3}/ Mn^{+4}(DE) double exchange , where (Mn^{+3} / Mn^{+4}) are non-integral valence medium materials (3).

William Thomson discovered the first magnetic resistance in 1856, where is (All metals have magnetic resistance, which varies when exposed to a magnetic field) (4)

The discovery of (colossal magnetoresistance) in the manganites with the perovskite structure has stimulated research on ferromagnetic metallic oxides (5,6).

In this study, the effect of Sr- doping in a formula $Pr_{1-x}Sr_xMnO_3F_y$ (x = 0.2, 0.3, 0.4 and 0.5) on the physical properties was investigated. In order to study the structure, the surface morphology and electrical and magnetic properties of the specimens, X-ray diffraction (XRD), scanning electron microscope (JEOL JSM6390LV SEM) and magnetoresistance at various magnetic fields as a function of temperature measurements were carried out, respectively. Then, the results of these measurements were discussed by comparing the other related materials.

1.1 Perovskite

Perovskite is a naturally (calcium titanate) mineral with the chemical symbol $CaTiO_3$ that was found in the Ural mountains (Russia) by German mineralogist Gustav Rose in 1839 and named the following "Russian mineralogist" Lev Perovsky (7,8)

Perovskite oxides inorganic such as ($CaTiO_3$, $LaMnO_3$, etc) have been studied extensively in recent decades due to their numerous uses in the fields of science and technology (optics, magnets, electronics, and superconductors).

Magnetic perovskite is one of the most exciting materials for scientific, technological, and commercial purposes because it is the most energy-efficient and inexpensive material used in many applications such as electronics and photovoltaics. For all these reasons, the focus is on modeling and investigating the magnetic properties of ABO_3 perovskite, Whereas the A and B sites contain cations and O ionic.

A: is a rare-earth element (Nd, Eu, Sm, Pr, Gd, etc).

B: is a transition metal element (Mn, Fe, Co, etc).

O: is oxygen.

Jonner and Van Santen were the first to study perovskite manganites. They discovered that changing the proportion of Mn^{+4} in $LaMnO_3$ by inserting bivalent alkaline earth metal elements (Ca, Sr, Ba) with varying doping ratios caused variations in the Curie temperature (T_C) and saturation magnetization ever since the name "manganites" has been used to mention the compounds that contain both trivalent and tetravalent elements (9).

1.2 Perovskite Structure

The crystal structure of perovskite was initially distinguished in 1926, by the Norwegian mineralogist Victor Goldschmidt in his study of 'tolerance factors.

Later, in 1945 the crystal structure was published by Irish crystallographer Helen Dick Megaw (1907-2002) based on x-ray diffraction data for (barium titanate).

Manganite with a (Perovskite structure) is an important class of oxides with thoroughly investigated Colossal Magnetoresistance (CMR) properties.

Perovskite material with the same structure as (Titanium oxide) and the mineral calcium the first perovskite crystal was discovered (10,11).

ABX_3 is the general formula for perovskite composites (fig 1.1), with A and B as cations and X as an anion.

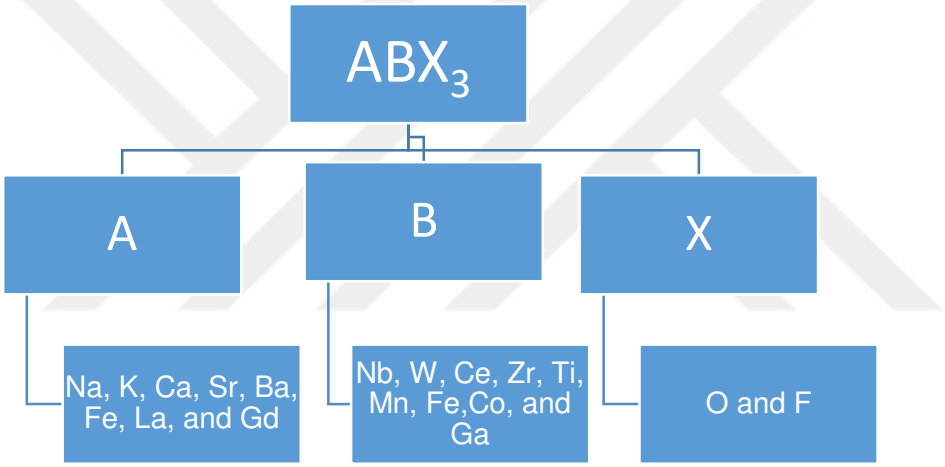

Fig1.1. The general formula for perovskite ABX3

Because of this formula and the flexibility of this structure, scientists could design perovskite crystals that contain many elements, forming various compounds with different electrical, optical, and physical properties. Today can find perovskite in multiple applications such as ultrasound devices, memory chips, etc.

The chemical formula ABO_3 (Picture 1.1) has been adopted for the perovskite structures of many oxides. The cubic form is an ideal structure with space group (Pm3m) No: 221, the orthorhombic with space group (Amm2) No: 68 or (Pnma) No: 62, and tetragonal with space group (I4/mcm) No:140 or (P4mm) No: 99, Non-cubic varieties are the most common.

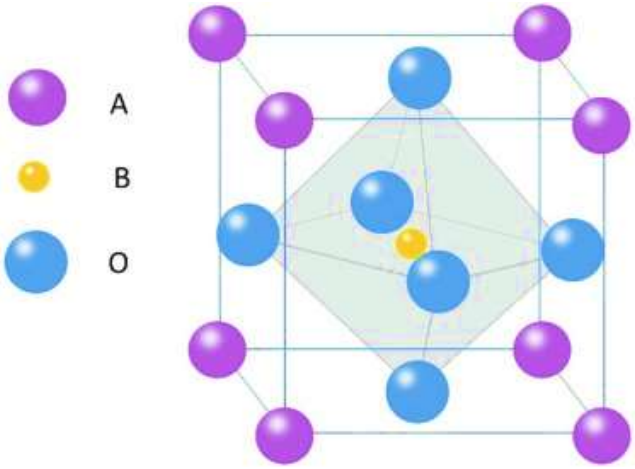

picture 1.1. A perovskite cube where the purple color is A cation, the yellow color is the B cation, and the blue color represents the oxygen anions.

Perovskite compounds have been well-known and widely used in a variety of applications for decades. It can be made in a variety of ways, such as the traditional solid-state reaction or co-precipitation technique, alkoxides hydrolysis, organometallic treatment, hydrothermal procedure, etc.

1.3 Goldschmidt Tolerance Factor

In "1926" Victor Moritz Goldschmidt presented the first explanation for the perovskite tolerance factor "t" to determine perovskite phase stability for a given collection of anions and cations of the ABX_3 crystal structure, by the eq:

$$t = \frac{(r_A + r_x)}{2(r_B + r_x)}$$

where (r_A, r_B, and r_X) are the ionic radius of A, B, and X. When the value of "t" is between 0.8 and 1.0, a stable perovskite structure is created. However, when the value of t is bigger than 1 or smaller than 0.8, a nonperovskite phase is generated (12).

For materials with a smaller tolerance factor, the symmetry is reduced. When t > 1, A cations are large and the B cations are small, allowing the B ions to move more freely. The B cations have a considerable size for t 1 and above. In reality, the ion packing in the perovskite cell is related to t. A perfect cubic cell is generated when the number (**t**)

equals one. When (**t**) differs from 1, the perovskite cell deforms and the symmetry is reduced.

1.4 Jan-Teller Effect

In 1937 was the first report about the Jan-Teller effect or sometimes called Jan-Teller (distortion). It's the geometric deformation of molecules and ions caused by certain electronic arrangements. This name was given after (Hermann Arthur Jan 1907-1979) and (Edward Teller 1908-2003), who proved that degenerate orbital molecules could not be stable using "group theory" since distortion lowers the total energy of the molecule (13).

It's an essential part of shattering molecular solid-state structures spontaneous similarity. It has far-reaching implications in a variety of domains, and it accounts for a range of stereochemistry information, crystallography, molecular physics, solid-state physics and spectroscopy. The octahedral complexes of transition metals frequently exhibit these features ion has 3 electrons in two "degenerate orbitals" as a result of the (d^9) electronic configuration, resulting in an additional deteriorated electron ground state.

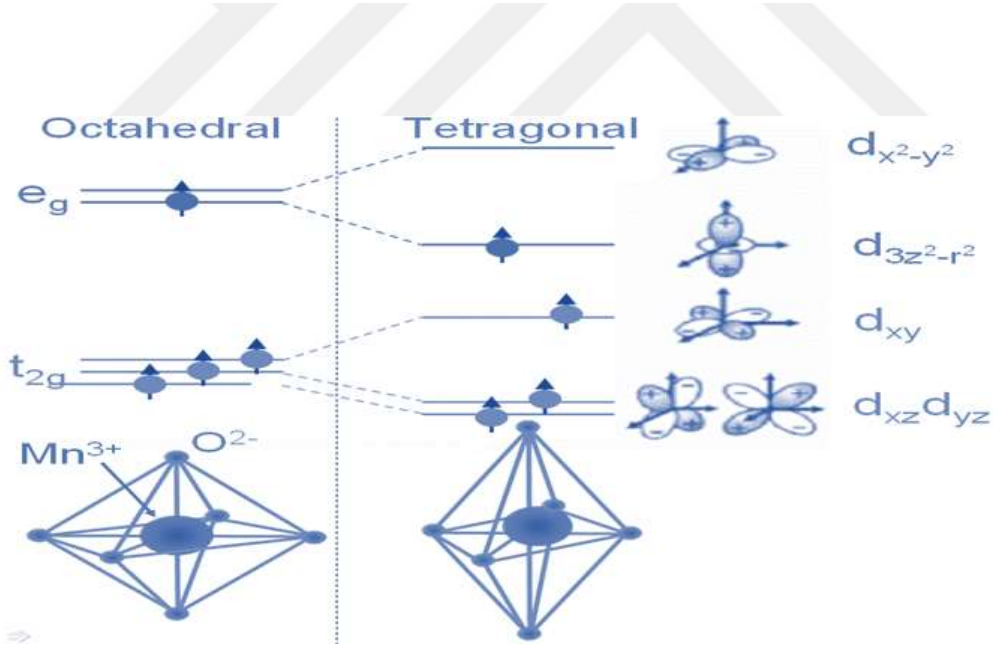

Fig1.2. The Jan-Teller Effect

These complexes deform along the (z-axis), reducing total energy, orbital and electronic degeneracy. The Jan-Teller effect (fig 1.2) simply predicts the presence of unstable component geometry, not the direction of the distortion. When this happens, electrostatic repulsion between both the primary Lewis ligand's electron pair and any

electrons in the (z) part orbitals is minimized decreasing the complex's energy inversion center. When (an odd number) of electrons occupy the e_g orbitals, the (JT) is most prominent in "octahedral" complexes. Compounds with the configurations d^9, low-spin (d^7) or high-spin (d^4), that have doubly degenerate ground states take this attitude.

More exactly, the effect happens when electrons in the t_{2g} orbitals degenerate. However, in these circumstances, the consequence is less dramatic because when the bonds are removed from the "t_{2g}" orbitals, which do not correspond directly to the bonds, there is a considerably lesser drop in repulsion. The same may be said for tetrahedral compounds like as (manganese). The distortion is mild since there isn't much stability to establish. The linkages, after all, don't link directly into orbitals.

1.5 Double–Exchange (DE)

The Double exchange first discussed by Clarence Zener (DE) is the magnetic interaction between two transition metal ions via oxygen ions and the ability to jump or position, reducing kinetic energy. As a result, this overall energy saving can lead to ferromagnetic alignment for neighboring metal ions transition.

Double exchange reactions, also called an exchange, double displacement reactions, or a double exchange chemical reaction, occur (when parts of two ionic compounds are exchanged, resulting in two new combinations).

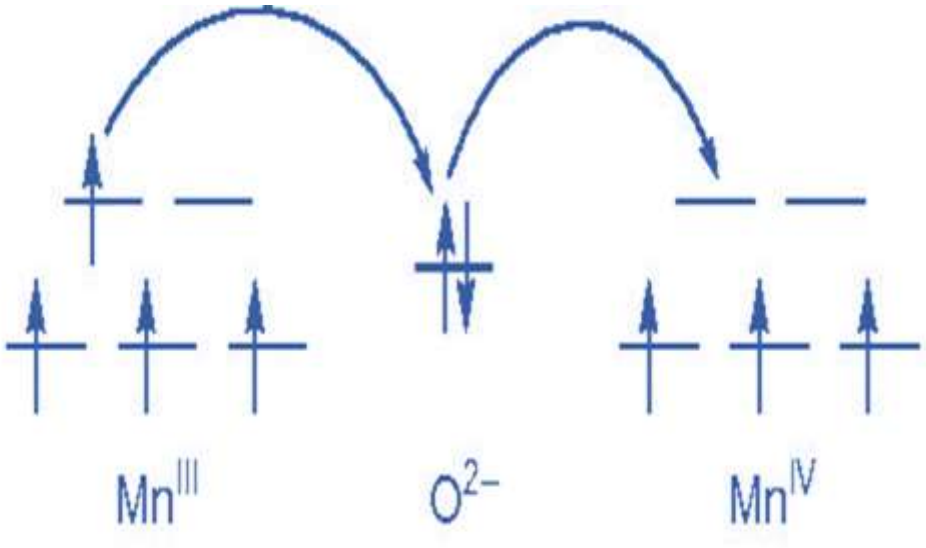

Fig1.3. A Double-exchange mechanism

More precisely, the effect occurs when degeneration occurs because of electrons in the t_{2g} orbitals. However, the result is less pronounced in these cases since there is a much lower reduction in repulsion when the bonds are taken away from the "t_{2g}" orbitals, this isn't a direct reference to the connection. The similar is true for tetrahedral complexes like (manganese). The distortion is very thin because there is lower stability to be obtained. after all the bonds do not point straight into the orbitals.

It occurs between two ions with no same balances or oxidation states that are linked through a non-magnetic element such as oxygen; in the fig 1.3 notes that in m^3 and m^4 there is a ferromagnetic interaction because the orbital moves through the levels, but there is no change in the orientation of spins.

More understandably, the double exchange reaction only happened when "one atom contains an extra electron compared to the other atom and is always ferromagnetic in nature and condition is both interacting metal ions should not have the same oxidation state.

1.6 Super Exchange

Hendrik Kramers proposed Super exchange in 1934 where he found that in crystals such as MnO, some Mn atoms interact with each other even though there are non-magnetic oxygen atoms between them. Less than two decades later, in 1950, Philip Anderson improved the Kramers model.

Super exchange or "Kramers–Anderson" super-exchange after his presenter, is usually strong "AFM" contact between two closer neighbor cations via a non-magnetic anion, and it's the outcome of the electrons being from the same donor atom and being paired with acceptor ion cycles, while if two adjacent positive ions are connected to the nearest neighbor at 90° to the non-magnetic bridge anion the reaction can occur ferromagnetic (FM) interaction.

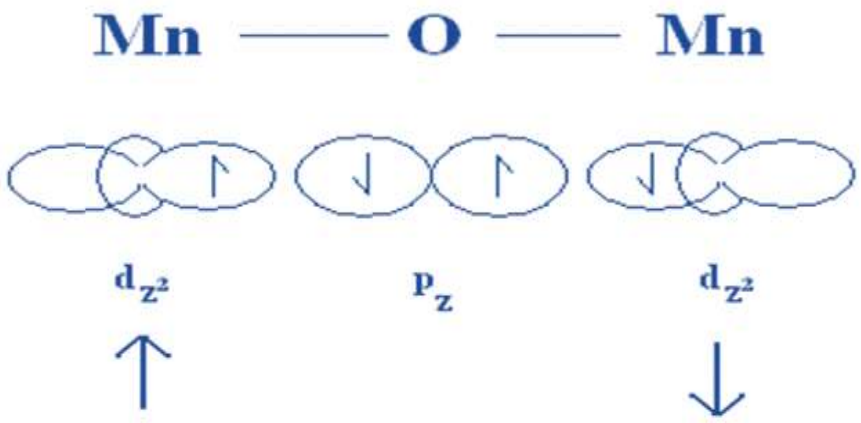

Fig1.4. Super Exchange

The difference between superexchange and double exchange is that in superexchange, occupancy of the metal ions' "d-shell" remains constant or varies by two, as well as the placement of the electrons is decided. The electrons in double exchange (DE) are wanderers (indeterminate), leading in materials with magnetic exchange coupling as well as magnetic exchange coupling (metallic conductivity).

Super-exchange is an indirect interaction between two magnetic cations via an intervening anion, O^{2-} (2p6) often as shown in Fig. 1.4.

1.7 The Ferromagnetic Materials

It is a certain group of materials that tend to appeared or display strong magnetism in the direction of field due to the application of an external magnetic field, the magnetic properties of these materials are mostly due to the alignment patterns of their component atoms. These atoms tend to behave like a simple electromagnet.

The bulk of magnetic materials is metals. Examples include iron, cobalt, nickel, and other magnetic materials. Metal alloys and rare earth magnets are also ferromagnetic materials.

It results from the oxidation of iron to iron oxide, which is a ferromagnetic substance. It has a temperature of 580°C Curie. Magnetite is the most attractive natural mineral on the planet.

It has a variety of qualities to mention them.

- Ferromagnetic atoms get sustained dipole moments in ranges.
- Atomic dipoles are orientated in the same way as the externally applied magnetic field.
- In the direction of the magnetizing field, the magnetic dipole moment is tremendous.
- When a ferromagnetic material is liquefied, it loses its magnetic properties with increasing temperature.

Once the magnetic field is removed, the material does not immediately demagnetize. To return the material to zero magnetization, a magnetic field in the opposite way should be applied.

Hysteresis is the ability of ferromagnetic materials to hold their magnetization once an external force is removed.

1.8 Magnetoresistance

The definition of this effect "Is the electrical resistance change of material when it exposed to an external magnetic field" and most of these materials are ferromagnetic.

There are various of effects that can be called (magnetoresistance); some of these effects occur in most non-magnetic metals and semiconductors, like Shubnikov–de Haas (SDH) oscillations, geometrical magnetoresistance, or positive magnetoresistance. And these are some of the effects that happen in magnetic metals, such as negative magnetoresistance in ferromagnetic material or anisotropic magnetoresistance (AMR).

The last kind happens in multilayer or multicomponent systems (magnetic tunnel junctions), colossal magnetoresistance (CMR), giant magnetoresistance (GMR), tunnel magnetoresistance (TMR), and extraordinary magnetoresistance (EMR).

The first discovery of magnetoresistance (MR) was in 1856 by the scientist William Thomson (Lord Kelvin), However, he could not reduce the electrical resistance of the material by more than 5%.

For materials featuring colossal magnetoresistance (CMR), resistance changes may appear by orders of magnitude. The effect is very low at room temperature but reaches about 50% at low temperatures in giant magnetoresistance (GMR) multilayer structures.

In recent years' studies have begun to reveal the effects of greater than 95% change in resistance in some perovskite systems (14).

1.9 PSMO System

Manganese oxide systems with a perovskite structure having a general chemical formula of $REMnO_3$ has been widely studied in both physics and applicability in recent decades (15-16) This system is an antiferromagnetic (AF) insulator (26) and after substitution into a specific ratio

$$RE_{1-x}AE_xMnO_3$$

Where RE: (La, Pr, Sm, Nd, etc) and A: (Ca, Sr, Ba, etc.)

Changing the doping levels of x as well as the relative and average sizes of R and A can alter the properties of manganese perovskites (15,18). These parameters are used to determine the anisotropic magnetic and transport properties of a single crystal perovskite manganite material (19,20). The distortion transforms into the ferromagnetic ordering state and metal-insulator transition occurs near the Curie temperature. The alkaline earth ion substitution causes significant phenomena observed in the structural, electrical, and magnetic features.

Praseodymium (Pr^{3+}) and strontium (Sr^{2+}) perovskite manganite materials with the mentioned formal above have gotten a lot of attention because of their peculiar characteristics and prospective applications.

The valence state of Pr is ($^{+3}$) and ($^{+4}$). These additional valence states are an excellent example of Hund's rule, which asserts that electronic levels that are empty, half-full, or filled are more stable.

Praseodymium-based manganite systems have become one of the most interesting compounds to investigate.

This is because of the interesting physical properties of this perovskite manganite, especially the compound with formula $Pr_{1-x}Sr_xMnO_3$, where its properties such as magnetic resistance and phase transition have attracted many researchers to delve deeper into its study and know its features.

2. EXPERIMENTAL

In this section, the details of the preparation of the perovskite manganite $Pr_{1-x}Sr_xMnO_3$ are described, following that, technical information regarding the measuring techniques and procedures used to determine the structural, electrical, and magnetic characteristics of the produced samples were provided.

Four samples of bulk ceramics manganese oxides in form $Pr_{1-x}Sr_xMnO_3$ (x= 0.2, 0.3, 0.4, and 0.5) (Table 2.1) have been prepared. Sample powders were mixed with high purity materials Pr_2O_3, SrF_2, MnO_3 (the Purity listed in table 2.2) using the traditional solid-state method by the steps listed in (fig 2.1). The stoichiometric ratio of powders (listed in table 2.3) was mixed thoroughly in an agate mortar and then calcined two times at 800 ºC for 12 h and 900ºC 24 h. The resulting mixture was crushed again and sintered twice at 1100 ºC and 1250 ºC for 24 hours. Finally, the pellets were slowly cooled to room temperature.

Table 2. 1.The Formulas of the samples

Compound formula	x	Samples
$Pr_{1-x}Sr_xMnO_3Fy$	0.2	$Pr_{0.8}Sr_{0.2}MnO_3Fy$
$Pr_{1-x}Sr_xMnO_3Fy$	0.3	$Pr_{0.7}Sr_{0.3}MnO_3Fy$
$Pr_{1-x}Sr_xMnO_3Fy$	0.4	$Pr_{0.6}Sr_{0.4}MnO_3Fy$
$Pr_{1-x}Sr_xMnO_3Fy$	0.5	$Pr_{0.5}Sr_{0.5}MnO_3Fy$

Table 2.2. The Purity ratio of the oxides that were used in the elaboration procedure. All chemicals are bought from the Alfa Aesar Company.

Compounds	Purity
Pr_2O_3	99.9%
SrF_2	99.9%
MnO_3	99.997%

Table 2.3. Stoichiometric calculations for $Pr_{1-x}Sr_xMnO_3F_y$ (x = 0.2, 0.3,0.4 and 0.5) compounds

Compounds	Pr_2O_3	SrF_2	MnO_3	$\sum_i M_i = 2.00\ g$
MW (g)	329.83	125.62	86.94	
0.2	1.19362	0.18078	0.62559	1.99999
0.3	0.96173	0.31396	0.72429	1.99998
0.4	0.83806	0.42558	0.73635	1.99999
0.5	0.82127	0.31279	0.86592	1.99999

- In the weight scale, we used 5 numbers after the comma

2.1 Solid-State Reaction

Chemical decomposition processes are used in this approach, in which a combination of solid reactants is heated to form a new solid and gaseous composition. Simple oxides, hydroxides, nitrates, carbonates, and other metal salts are commonly utilized to make complicated oxides.

This procedure usually entails a series of plasticizing steps followed by a series of intermediate grinding operations to improve the homogeneity of the mixture and lower the size of the powder particles. Furthermore, grinding the material improves the suitability of the powder for further heat treatment operations (sintering). Because it does not require complex but basic tools such as (agate mortar), the solid-state approach is reasonably affordable.

The samples were mixed according to calculated proportions to observe the effect of an increase in A-site. The resulting samples were mixed and crushed with the help of agate mortar. Pressed to reduce the surface area of powders. The first samples were sintered at 800 °C. The sintered samples were prepared at 1250 °C for measurement for the sample atoms to homogenize well.

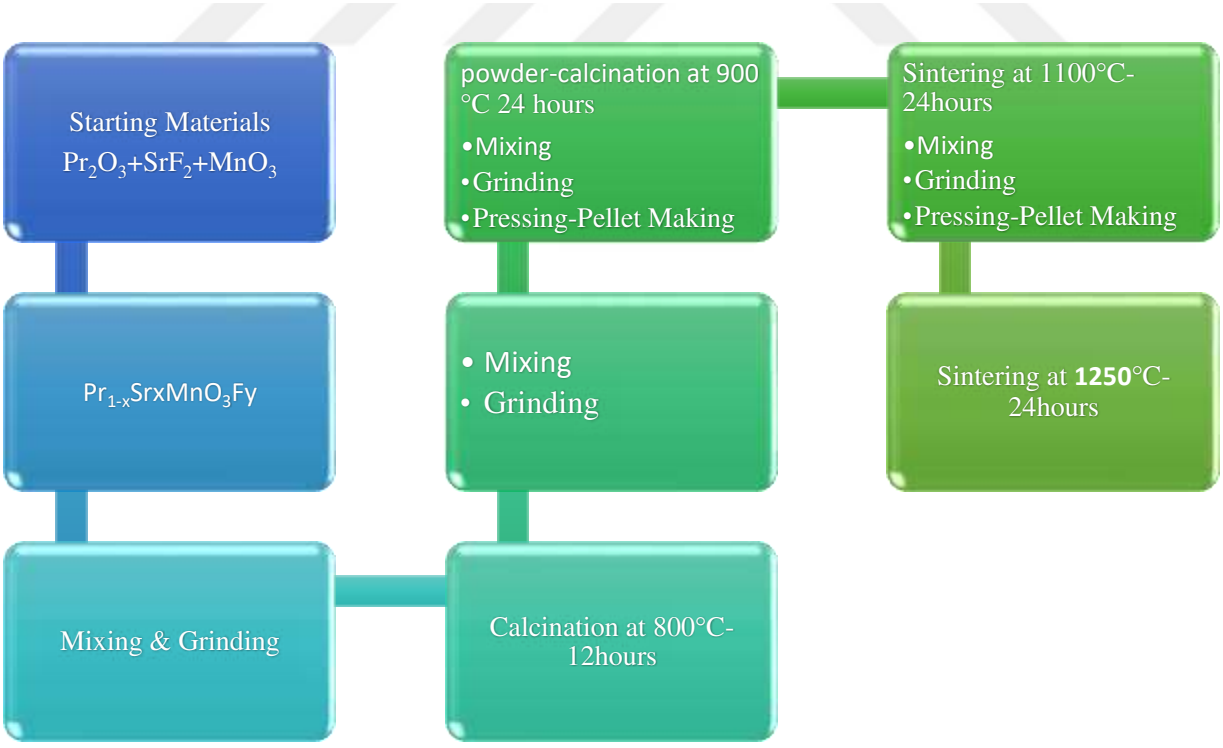

Fig 2.1. Steps of Solid-State Reaction

2.2 XRD, SEM and MR Measurements

The phase purity and structure of the samples were inspected by powder X-ray diffraction (XRD) at room temperature. The X-ray patterns were recorded with a Rigaku Multiflex diffractometer utilizing Cu-Kα radiation (λ=1.5418 Å) and scanning over the angular range of 20–80 degrees in Picture 2.1. Substantiation of the crystal structure and refining the unit cell parameters, The Jana 2006 program was used to perform Rietveld structural improvements.

Picture 2.1. Rigaku Multiflex X-Ray Diffractometer

The microstructure, surface morphology, and chemical content of the samples were studied utilizing scanning electron microscopy (SEM, JEOL 6390-LV) and an energy dispersive X-ray (EDX) spectrometer incorporated into the SEM as exhibited in Picture 2.2.

Picture 2.2. Scanning Electron Microscope JEOL 6390-LV

The electrical resistivity properties were determined as a function of temperature under 0 and 1T magnetic fields using a He-gas contact cryocooler and integrated into a superconducting coil magnet by the standard four-probature range of 30K-300 K as displayed in Picture 2.3.

Picture 2.3. He-gas contact cryocooler and integrated into a superconducting coil magnet

3. RESULTS AND DISCUSSION

Manganites present strong correlations between structural and physical properties. This correlation has been explained by both superexchange (SE) and double-exchange (DE) interactions between Mn^{3+} and Mn^{4+} ions. It is also well-known that the DE interaction between Mn^{3+} and Mn^{4+} ions alone cannot explain the behaviours observed in manganite systems. Thus, many studies suggest that it is necessary to rely on the average A-site cationic radius $\langle r_A \rangle$ (20,21) the oxygen content [22], and the synthesis temperature [23-25].

The $Pr_{1-x}Sr_xMnO_3$ (PSMO) series show a large ferromagnetic domain extending from x = 0.2 to x = 0.5. This system belongs to the large bandwidth manganites family and shows remarkable magnetoresistance values. Moreover, the PSMO systems are easy to fabricate, and their cost is relatively low compared to other manganite systems showing similar behaviours. In this study, we carried out a detailed study of the structural and magneto-electrical transport features of $Pr_{1-x}Sr_xMnO_3F_y$ (x = 0.2, 0.3, 0.4, and 0.5) ceramics.

3.1 X-ray Diffraction

It is clear from the results of the refinement that all the samples show the characteristic peaks of the perovskite structure with no observable inclusions and samples crystallized in a single phase with an orthorhombic structure and a Pnma space group (N:62). It should be noted here that a second phase with I41/AMD space group (N:141) is observed for the $Pr_{0.5}Sr_{0.5}MnO_3$ sample. The gathered structural results such as cell parameters, unit cell volume, the attained quality (R_P, R_{WP}) factors, and the goodness of fit (GOF) are listed in Table 3.1. The inset graphs of the XRD patterns indicate that the main diffraction peak (32.51) shifts to lower angles which is a sign of the expansion in the cell volume.

It is seen in Table 3.1 that the cell parameters decrease with increasing Sr concentration. This can be attributed to the decreasing the content of Mn^{+3}/Mn^{+4} ratio. As the Sr^{+2} content increase, the formation of Mn^{+4} ions also increases. Since the ionic radius of Mn^{+4} (0.53 Å) is lesser than Mn^{+3} (0.645 Å), one would expect the decrement in the cell parameter as x-rise.

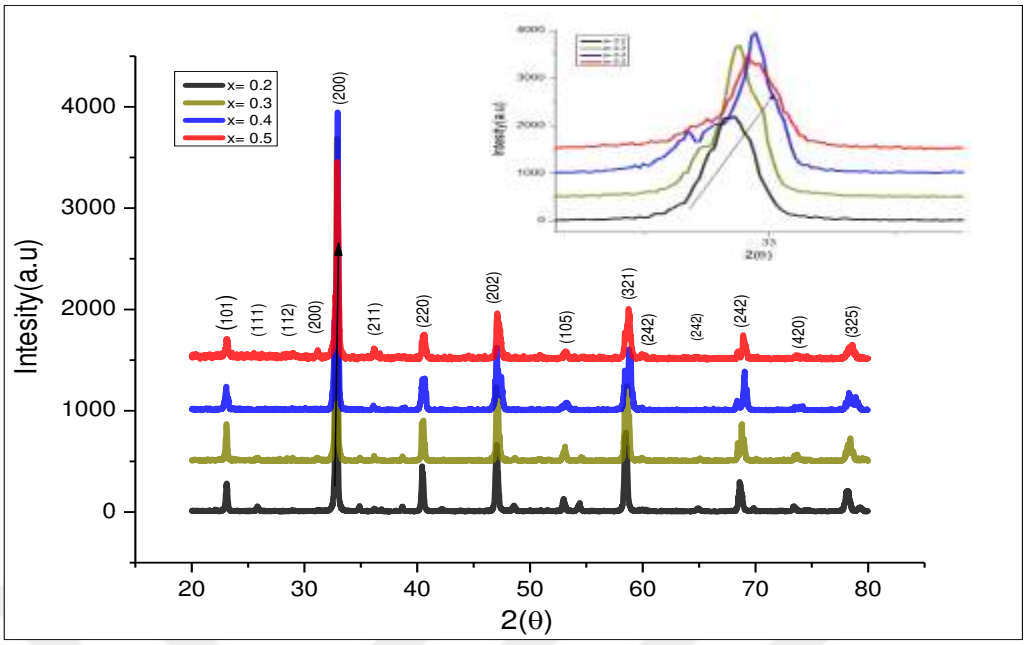

Fig 3.1. The x-ray diffraction pattern for $Pr_{1-x}Sr_xMnO_3F_y$, x= (0.2, 0.3,0.4 and 0.5) Inset shows extended view of the same pattern at 32-33° angles.

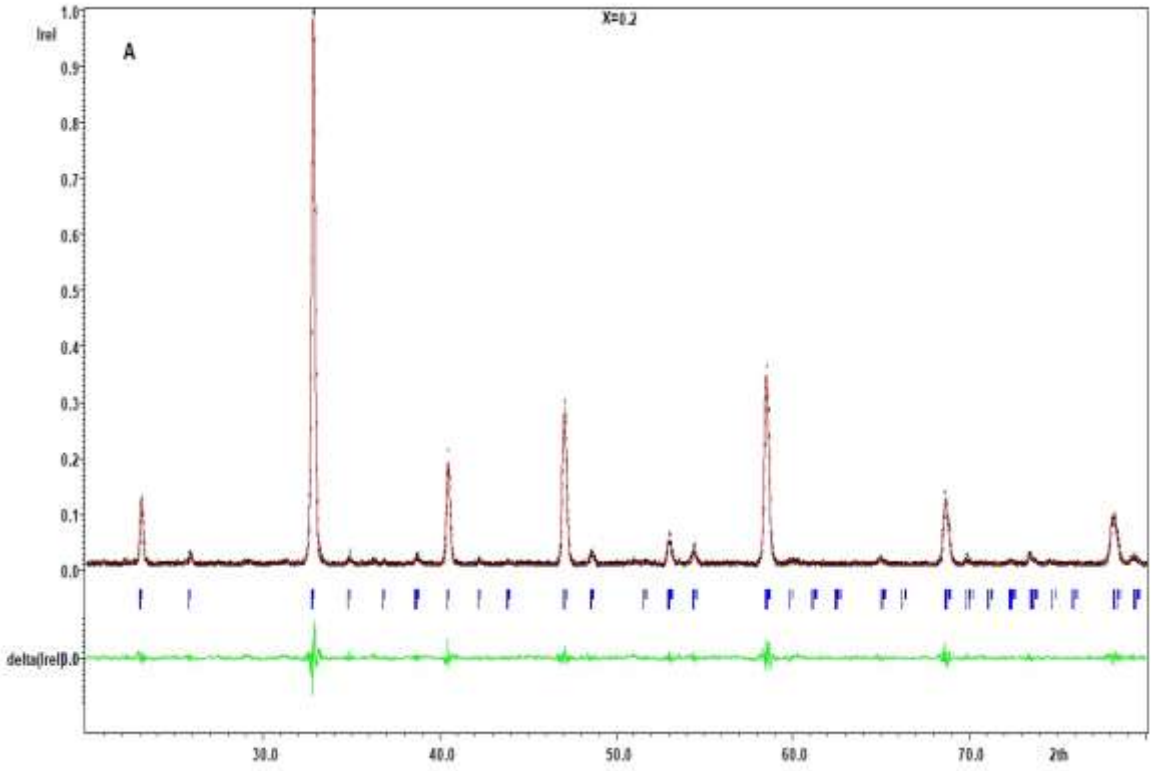

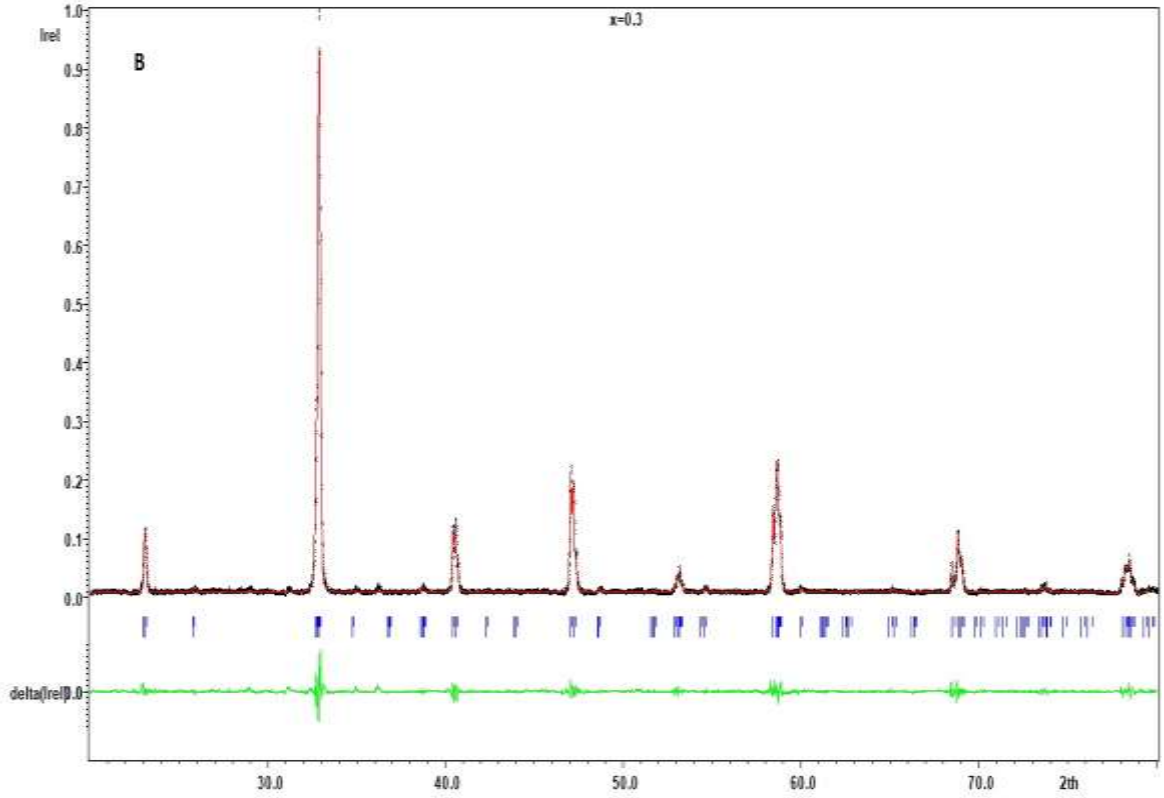
x=0.3
B
Inel
delta(Inel)
30.0
40.0
50.0
60.0
70.0
2th

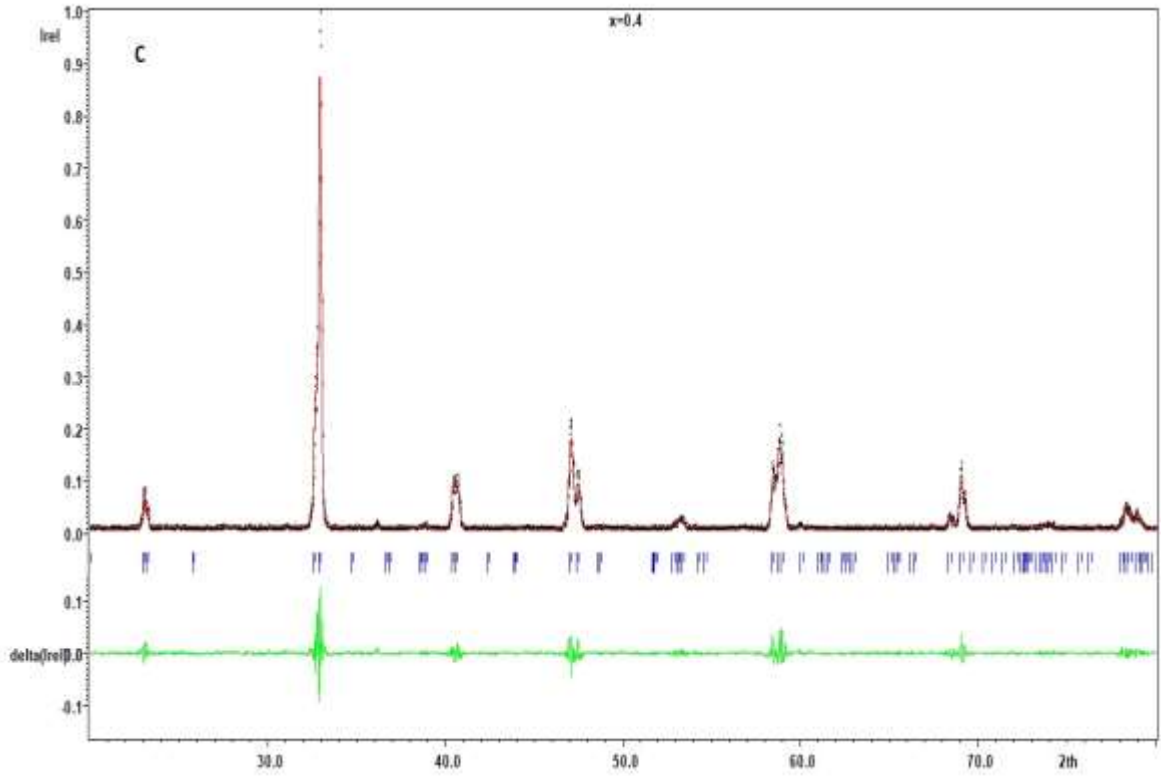
x=0.4
C
Inel
delta(Inel)
30.0
40.0
50.0
60.0
70.0
2th

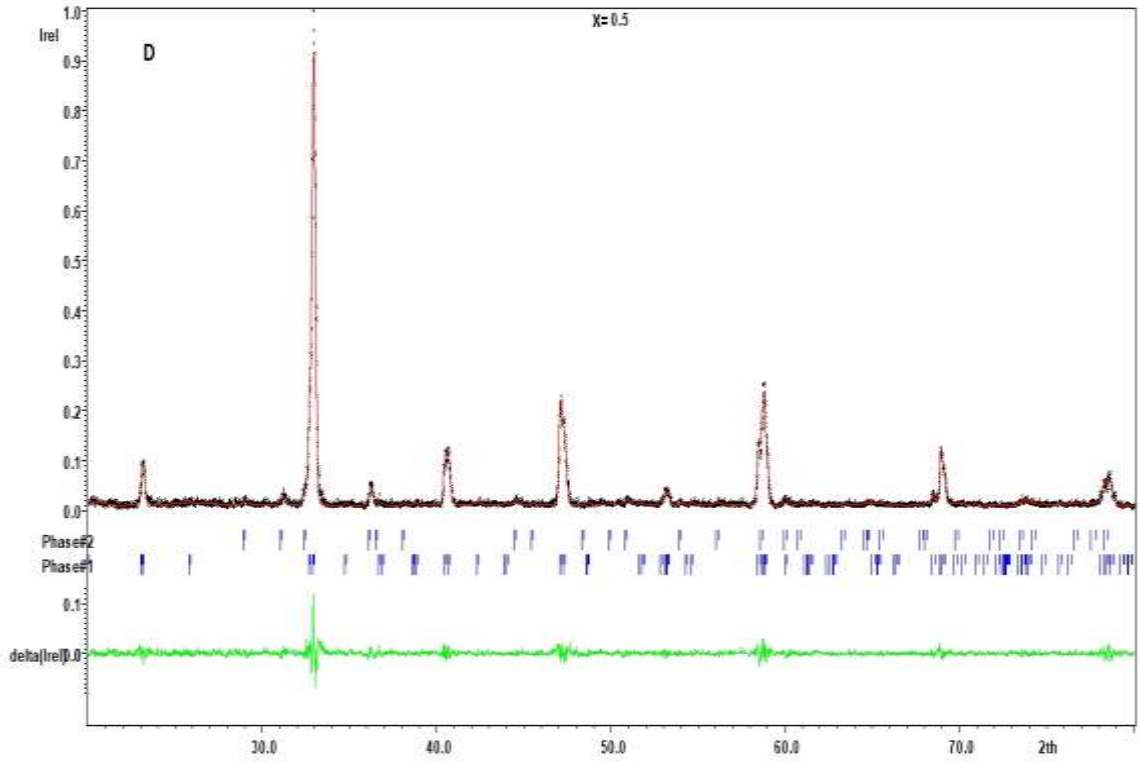

Fig 3.2. Xrd refinement for (a) $Pr_{0.8}Sr_{0.2}MnO_3F_y$, (b) $Pr_{0.7}Sr_{0.3}MnO_3F_y$, (c) $Pr_{0.6}Sr_{0.4}MnO_3F_y$ (d) $Pr_{0.5}Sr_{0.5}MnO_3F_y$, the experimental data are plotted with the red cross line, the calculated pattern is plotted with the black solid line. The difference plot between the observed and the theoretical patterns is shown with the green line.

Table 3.1.The structural parameters for $Pr_{1-x}Sr_xMnO_3$ with (x=0.2, 0.3, 0.4, and 0.5) samples.

$Pr_{1-x}Sr_xMnO_3$				
X	**0.2**	**0.3**	**0.4**	**0.5**
Space group	**Pnma**	**Pnma**	**Pnma**	**Pnma,I41/AMD**
a (Å)	5.466	5.444	5.442	5.479
b (Å)	5.461	5.475	5.486	5.439
c (Å)	7.710	7.695	7.666	7.684
V $(Å)^3$	230.160	229.413	228.938	229.071
GOF	**0.51**	**0.63**	**0.70**	**0.80**
Rp	7.37	8.59	10.31	12.00
w_{RP}	10.16	1182	12.96	16.50
D (nm)	38.28	40.86	45.03	36.38
GrainSize(μm)	4.02	1.5	1.86	2.10
t	0.810	0.814	0.818	0.823
σ^2	1.743	1.784	1.827	1.870

The tolerance factor *t* that an important parameter related to the structural symmetry of perovskites and significantly affects the electron transport properties we can find out the value of the coefficient t through the equation defined by Goldschmidt

$$t = \frac{r_A + r_O}{\sqrt{2}(r_B + r_O)}$$

where r_A, r_B, and r_O are the ionic radii of A-site, Mn (B-site), and O ions respectively, and $r_i = \sum_0^i yiri$. The average ionic radius $\langle r_i \rangle$ values and tolerance factor *t* of our samples are calculated and listed in Table 1. The ionic radii of all the used elements are 1.29 Å, 1.45 Å, 0.645 Å, 0.53 Å, and 1.35 Å of the elements (Pr^{3+}, Sr^{+2} Mn^{3+}, $Mn^{4+,}$ and O^{2-} respectively), which according to the coordinate number of 12 for Pr, Sr, 6 for Mn and anions. With the replacement of the larger radius Sr^{+2} ions with the smaller Pr^{+3} ion, an increase in the *t* value was observed.

we valuation the average crystallite size, "D" by using the Scherrer formula;

$$< D >= k\lambda / \beta \cos\theta$$

where *k* is the shape factor generally equal to 0.9 for spherical crystals, λ is the wavelength of the X-rays (λ = 1.5418 Å), θ is Bragg's angle and β is the full width at half maximum of peaks. The estimated crystallites size is found to be in the range of 36.38 nm and 45.03 nm.

3.2 Scanning Electron Microscope

The SEM micrographs demonstrate that all the samples have a granular morphology and the average grain sizes are observed to decrease with increasing Sr-content (from 4.02 to 2.10 μm) as the grains size distribution histograms scale adjustment with gaussian function. It is clear from the sem images that all samples have identical surface topography from the point of view and x=0.2 and x=0.5 samples have denser surface morphology.

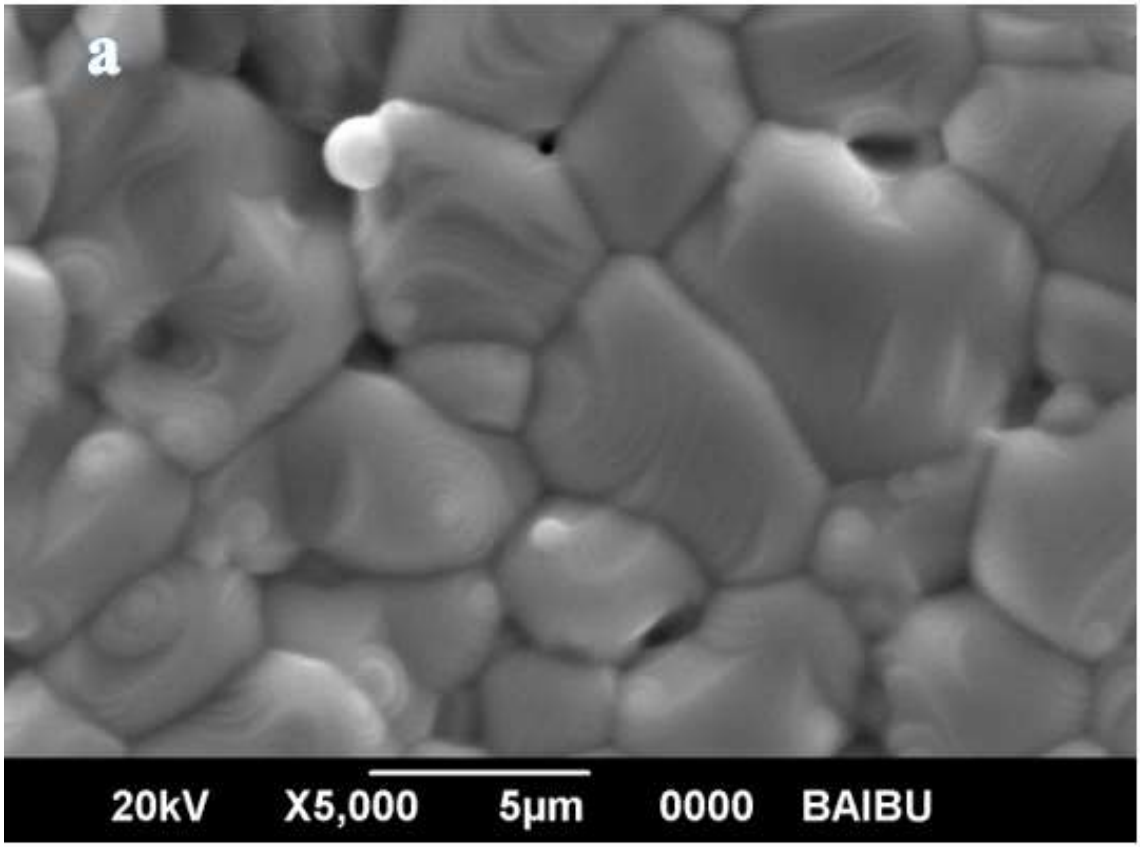

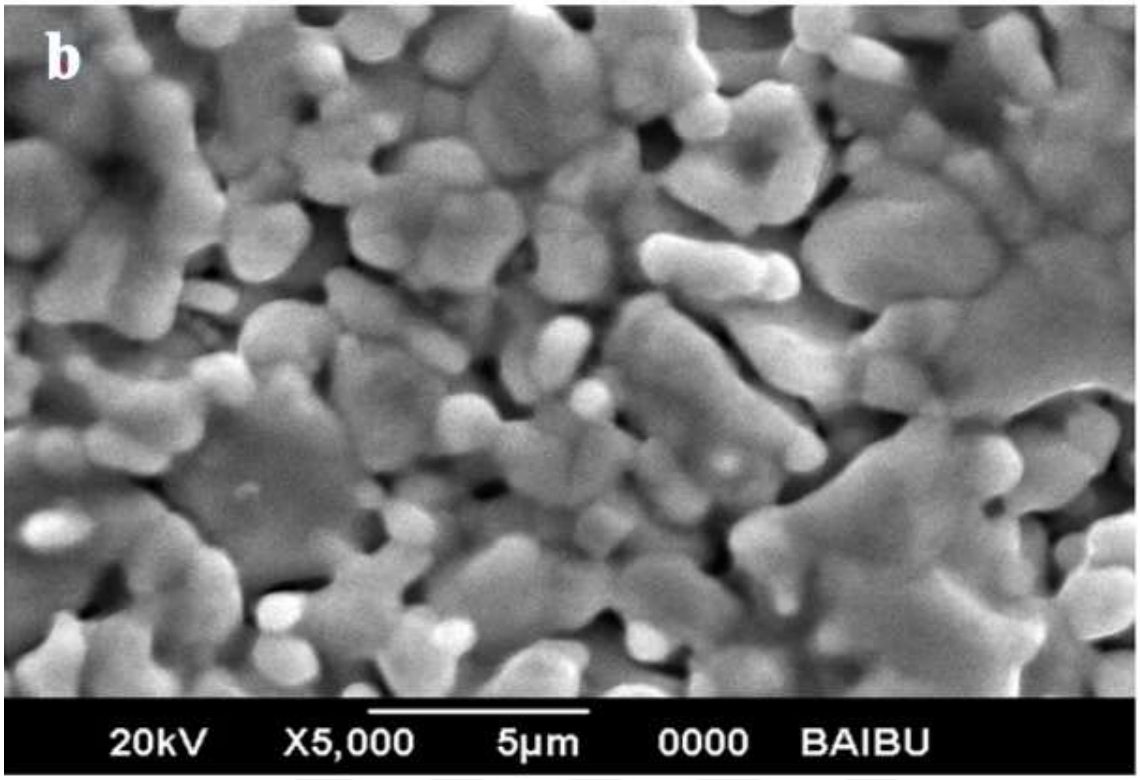
b
20kV X5,000 5µm 0000 BAIBU

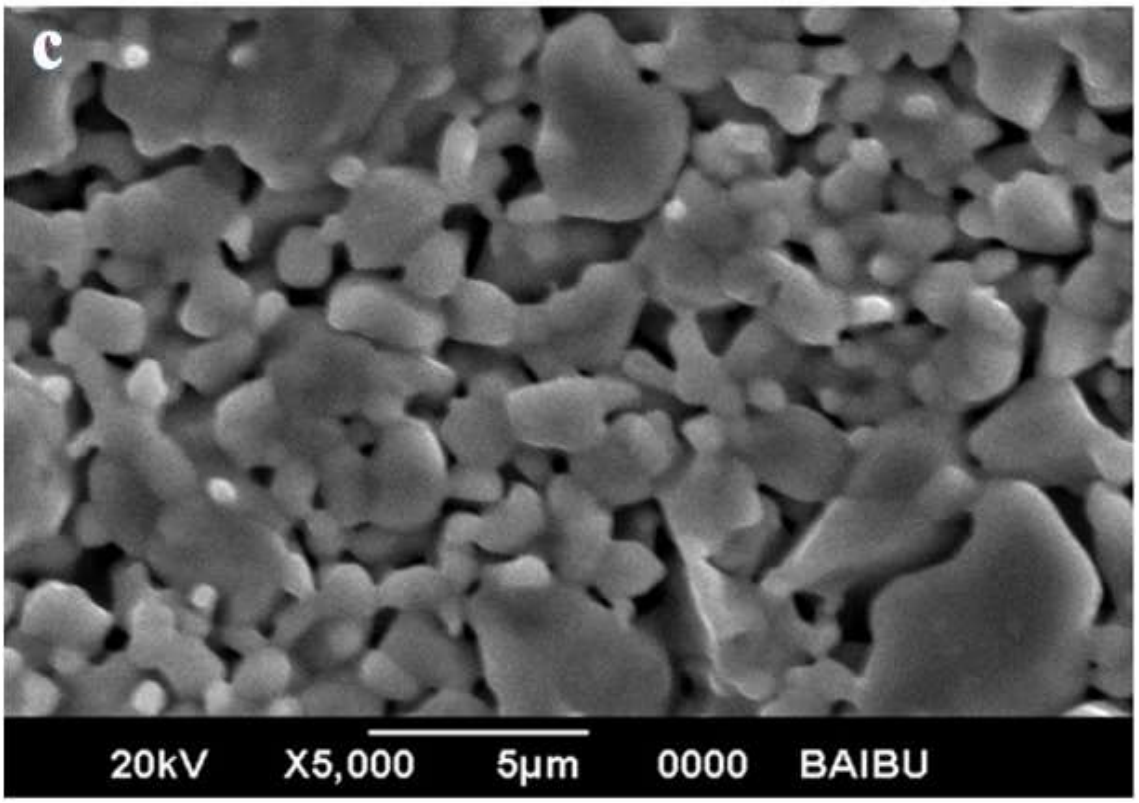
c
20kV X5,000 5µm 0000 BAIBU

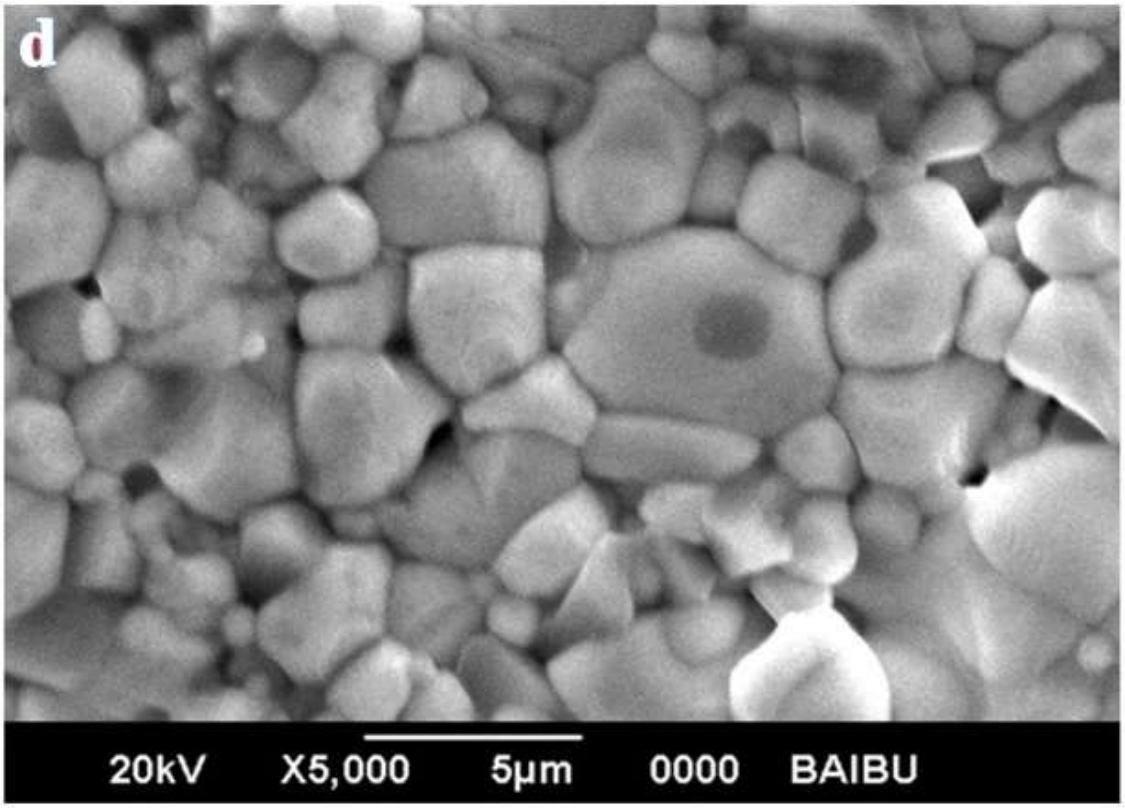

Fig3.3. SEM micrographs of compounds with (a)$Pr_{0.8}Sr_{0.2}MnO_3F_y$ (b) $Pr_{0.7}Sr_{0.3}MnO_3F_y$ (c) $Pr_{0.6}Sr_{0.4}MnO_3F_y$ (d) $Pr_{0.5}Sr_{0.5}MnO_3F_y$.

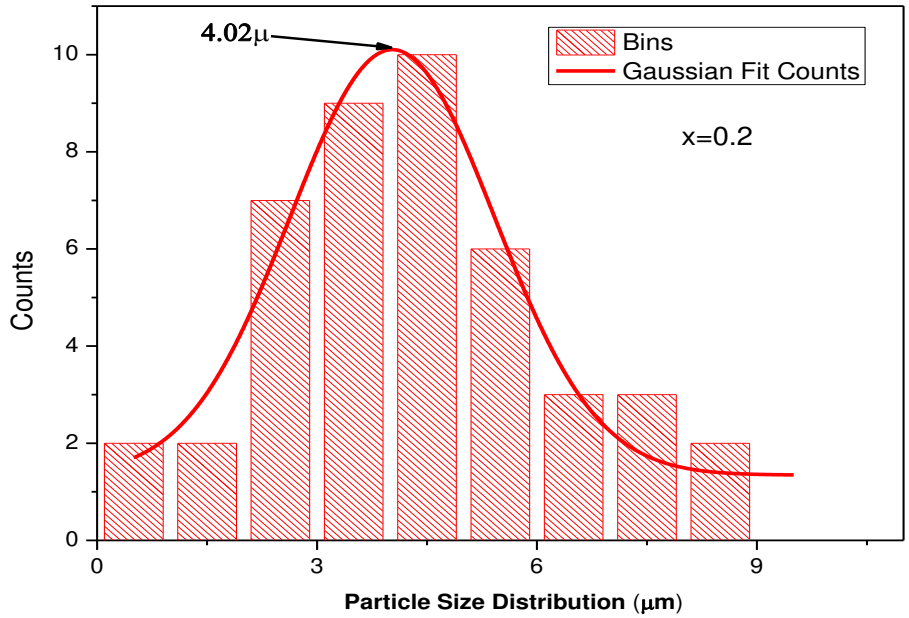

Fig3.4 Size distribution graph for $Pr_{0.8}Sr_{0.2}MnO_3Fy$ from the SEM image.

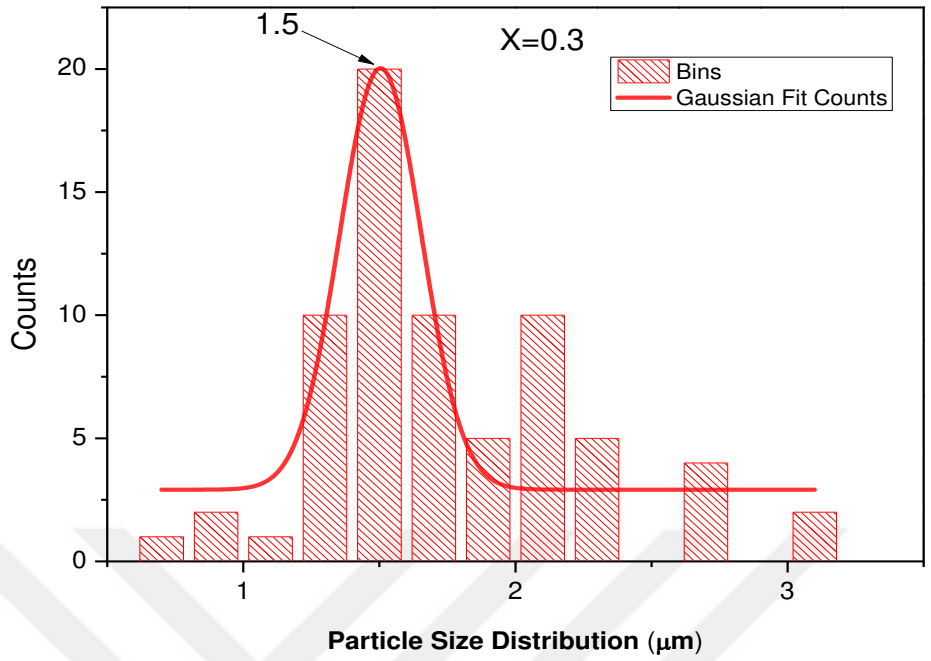

Fig 3.5 Size distribution graph for $Pr_{0.7}Sr_{0.3}MnO_3F_y$ from the SEM image

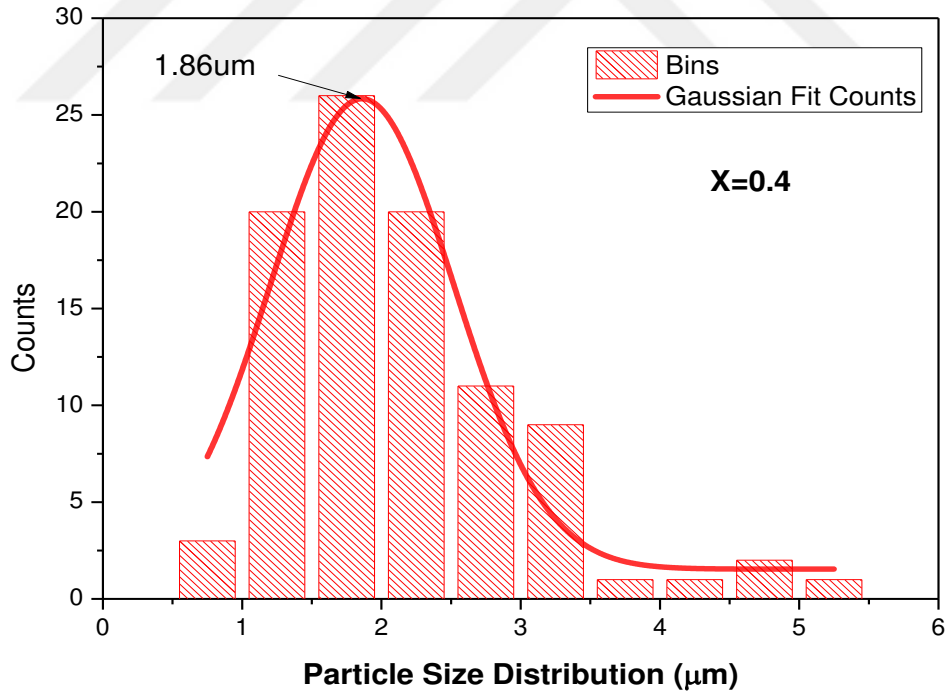

Fig 3.6 Size distribution graph for $Pr_{0.6}Sr_{0.4}MnO_3Fy$ from the SEM image.

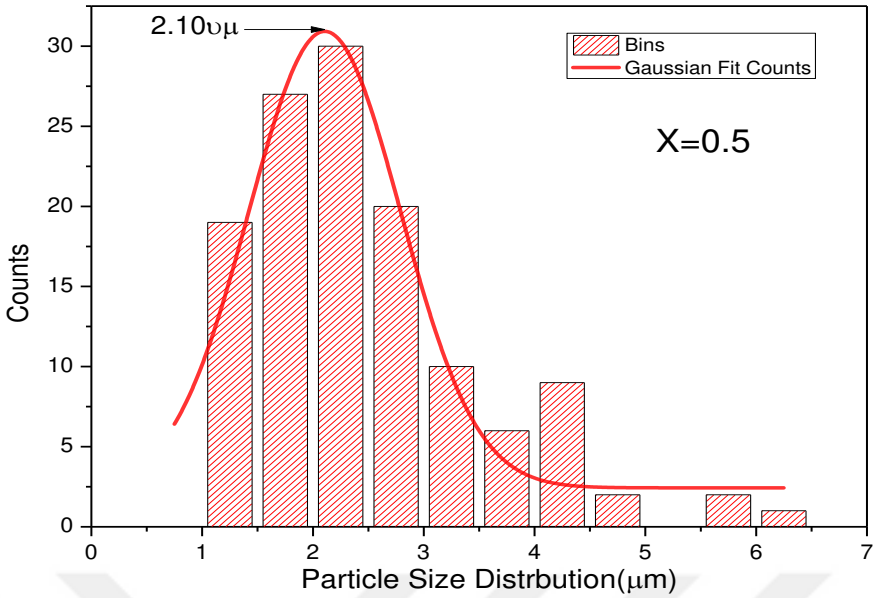

Fig 3.7 Size distribution graph for $Pr_{0.5}Sr_{0.5}MnO_3Fy$ from the SEM image.

3.3 Electron Dispersive X-Ray

The EDAX spectra of all perovskite samples are shown in Fig. 3.8 It is clear that all samples contained predicted components with no significant extra impurities. In addition, semi-quantitative EDAX analysis corroborated the relative atomic ratios of all elements near the predicted elements and is listed in Table 3.2.

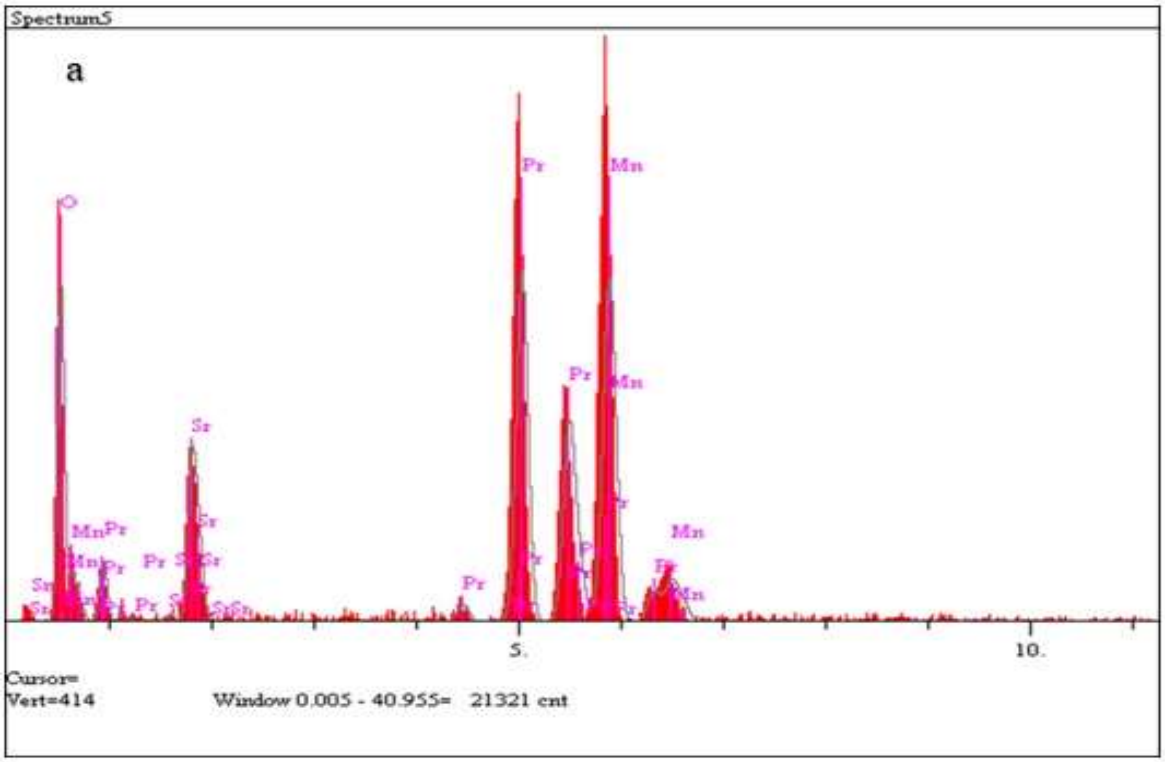

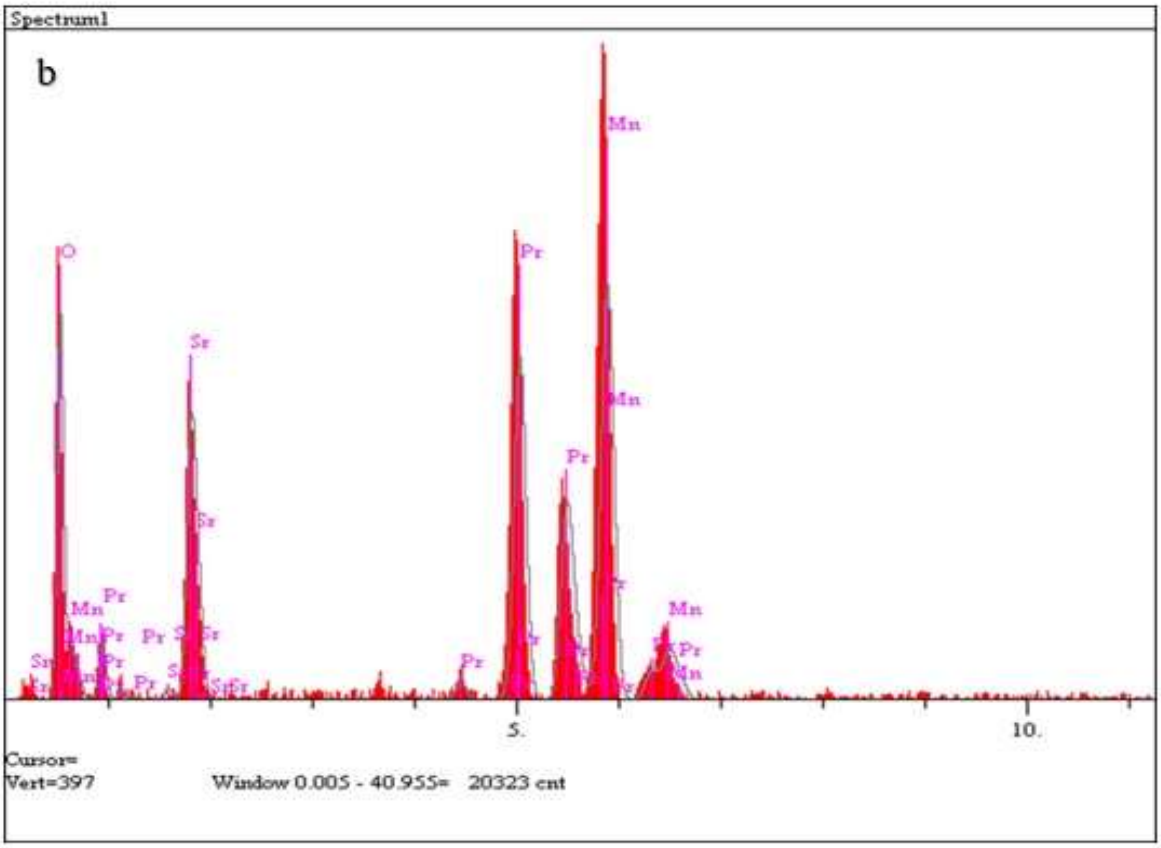
Spectrum1
b
Mn
O
Pr
Sr
Mn
Pr
Pr
Mn
Pr
Mn
Pr
Mn
5.
10.
Cursor=
Vert=397
Window 0.005 - 40.955= 20323 cnt

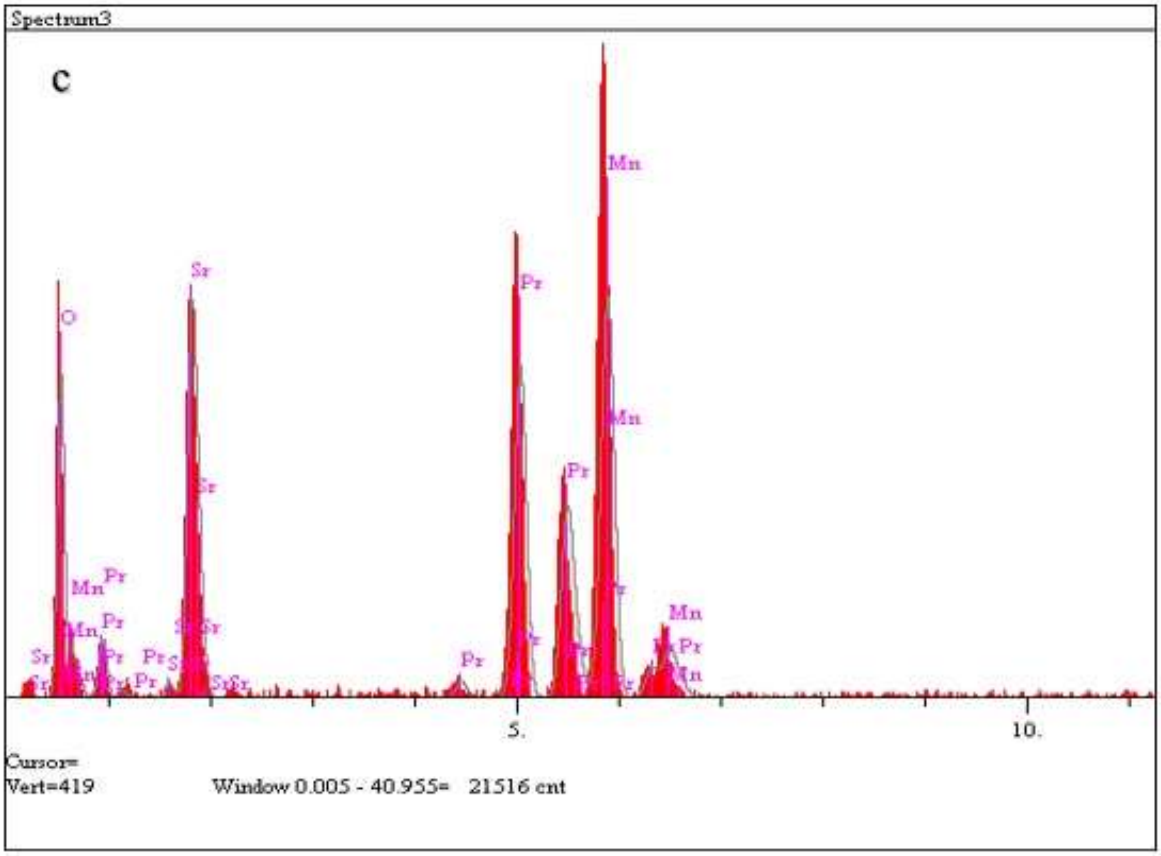
Spectrum3
c
Mn
Sr
O
Pr
Mn
Pr
Sr
Mn
Pr
Mn
Pr
Mn
5.
10.
Cursor=
Vert=419
Window 0.005 - 40.955= 21516 cnt

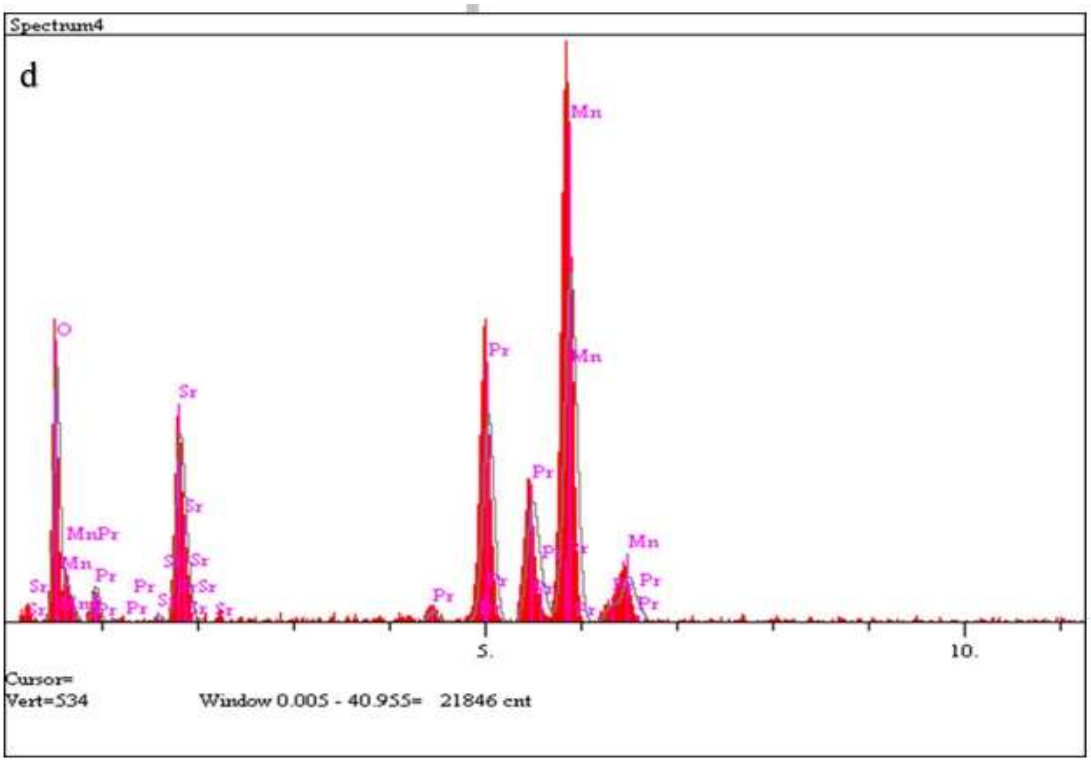

Fig 3.8. Electron dispersive x-ray analyses (a) $Pr_{0.8}Sr_{0.2}MnO_3F_y$ (b) $Pr_{0.7}Sr_{0.3}MnO_3Fy$ (c) $Pr_{0.6}Sr_{0.4}MnO_3Fy$ (d) $Pr_{0.5}Sr_{0.5}MnO_3F_y$.

Table3.2 The results of Electron Dispersive X-Ray Analyses

Elements	**Line**	**Concentration (wt.%)**			
		X=0.2	**X=0.3**	**X=0.4**	**X=0.5**
O	Ka	22.312	23.761	21.284	24.554
Mn	Ka	12.118	13.430	12.769	17.439
Sr	La	12.431	17.011	22.512	17.853
Pr	La	53.139	45.798	43.435	40.154
Total		**100**	**100**	**100**	**100**

3.4 Electrical transport studies

Magneto-electrical transport features are checked by the standard four-probe technique. In Fig. 3.9, we depict the resistance variation of temperature for all prepared ceramic materials within a long temperature range of 30-320 K in 0 T. When the measurement temperature is increased, all samples showed a significant hump which corresponds to metallic to insulating transition at the maximum resistivity temperature (T_{MI}). As the Sr content increases, the transition temperature increases monotonously with a general decrease in the electrical resistivity. Sr substitution remarkably affects the electric transport features in CMR manganites which can be seen by the significant shift of T_{MI} from 202 K to 313 K for x=0.3 and 0.5 samples, respectively.

It can be observed that the maximum resistivity ρ_{max} reduction and T_{MI} shifts to higher temperatures as the magnetic field increases. The shift of Tρ can be elucidation by the increase of alignment of magnetic moments which favors the delocalization of e_g electrons and leads to the improvement of DE interaction between Mn^{3+} and Mn^{4+} ions. Consequently, the FM metallic character will be enhanced. In fact, a higher applied magnetic field provides a higher electron hopping prospect that increases the FM domains and reduces the paramagnetic (PM) ones present in the structure. Thus, the FM metallic phase will be improved, and the resistivity will be reduced.

In samples with Sr content x =0.5 the FM transition temperature is found to decrease slightly to $T_C \sim$ 300K and the transition width also increases.

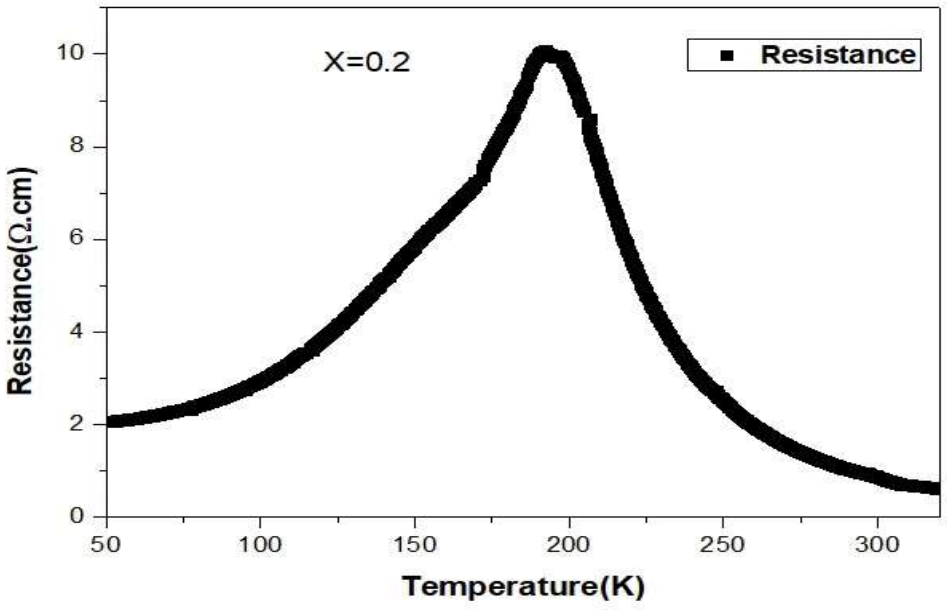

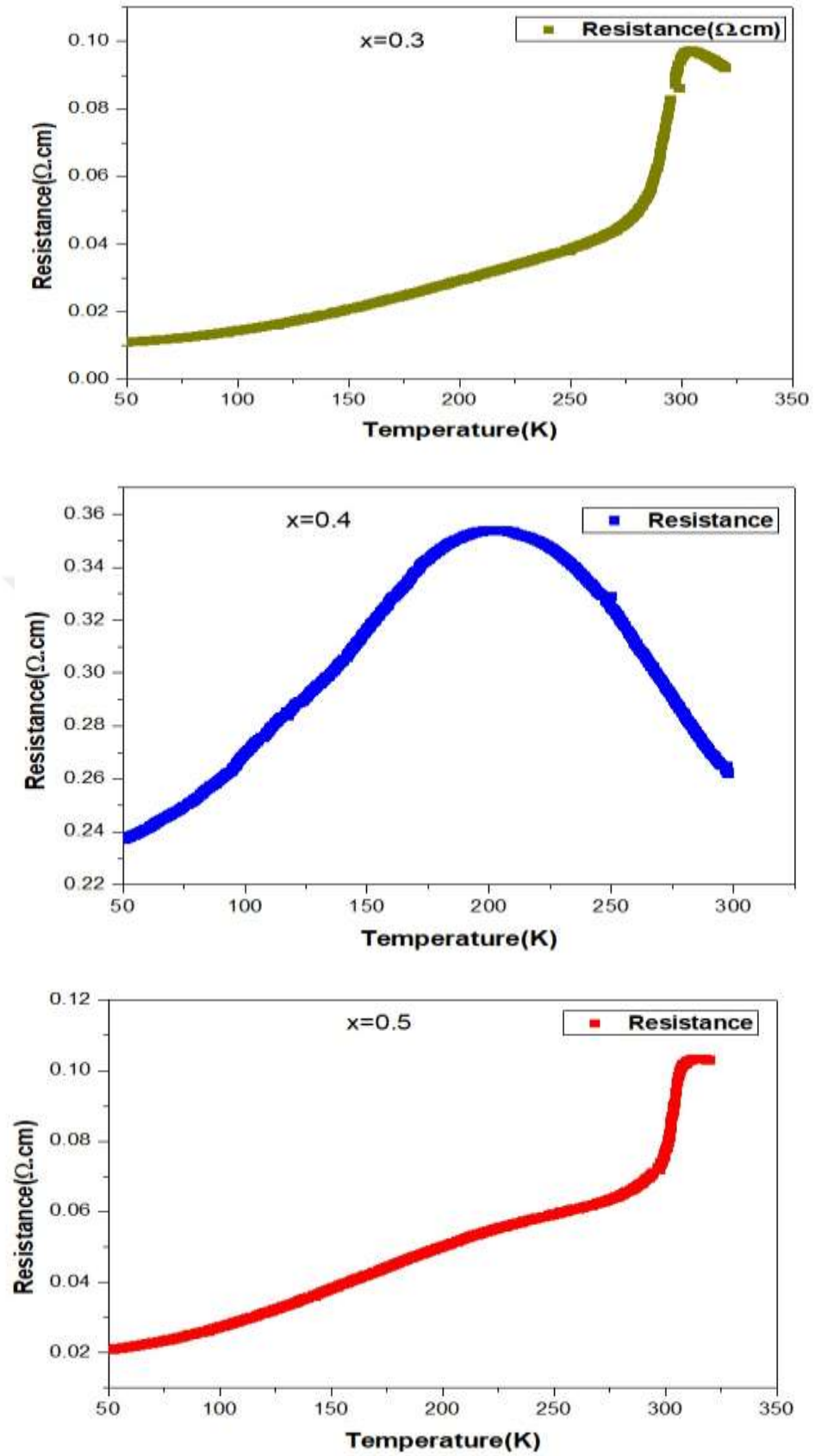

Fig 3.9 Resistance variation of temperature for he $Pr_{1-x}Sr_xMnO_3F_y$, x= (0.2, 0.3,0.4 and 0.5)

To deeply investigate the influence of magnetic field on magnetoresistance (MR), we calculated the MR % values, and their temperature dependence is shown in the insets of Fig. 3.10. During the magnetization process, the resistivity of the sample can change substantially. The relative change concerning the value under zero magnetic field can be characterized by the quantity so-called MR %, and quantified by the following formula:

$$\boldsymbol{MR}\ \% = \left[\frac{(\boldsymbol{\rho_H} - \boldsymbol{\rho_o})}{\boldsymbol{\rho_o}}\right] * \mathbf{100}$$

where ρ_0 and ρ_H are the resistivities at the applied magnetic field of zero and 1 T, respectively.

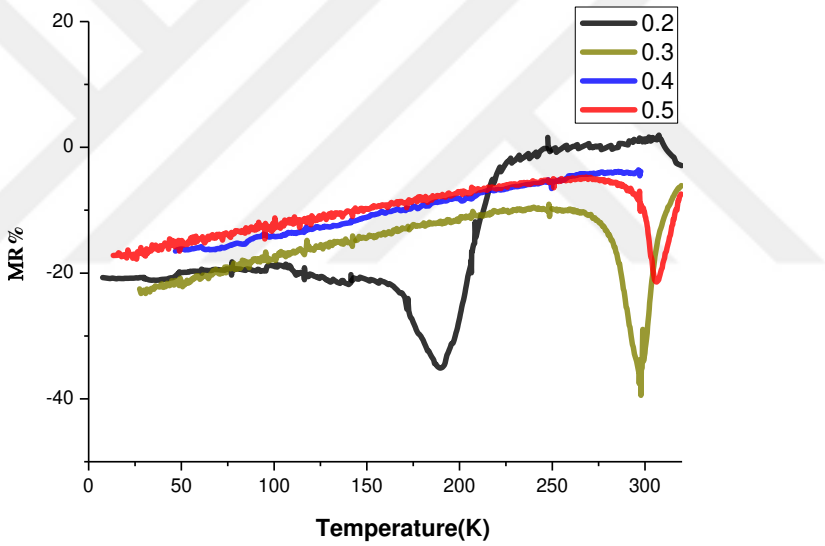

Fig 3.10. MR % with temperature dependence of the $Pr_{1-x}Sr_xMnO_3F_y$, x= (0.2, 0.3,0.4 and 0.5)

The effect of temperature on magnetoresistance percentage values is plotted in Fig.3.10 All the MR % vs T curves showed a similar variation trend, and Sr content exhibits a significant impact on the magneto-transport features of the PSMO system. As increasing Sr content, the maximum MR% value remarkably decreases, and corresponding maximum MR temperatures gradually increased. Noticeably, the MR% value decreased from 39 % to 4 %, and the maximum MR temperature increased from 191 to 313 K (Table 3.3).

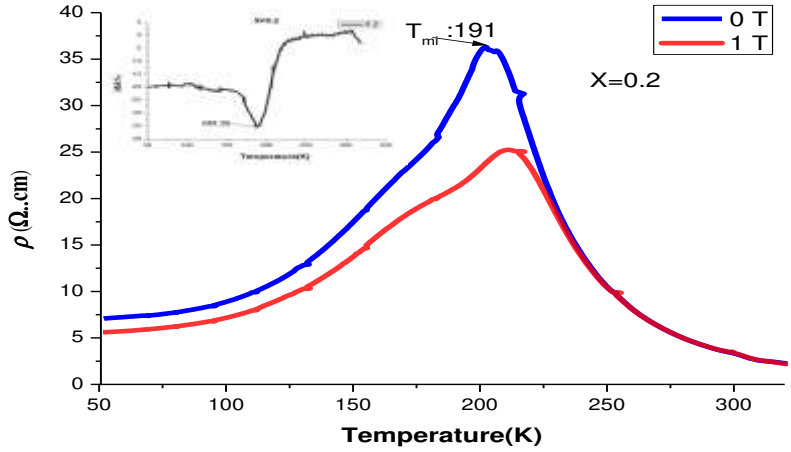

Fig 3.11 Resistivity dependence (ρ) on temperature graph for $Pr_{0.8}Sr_{0.2}MnO_3F_y$ sample under 0 and 1T magnetic fields. Included graph for MR % with temperature dependence on the same sample.

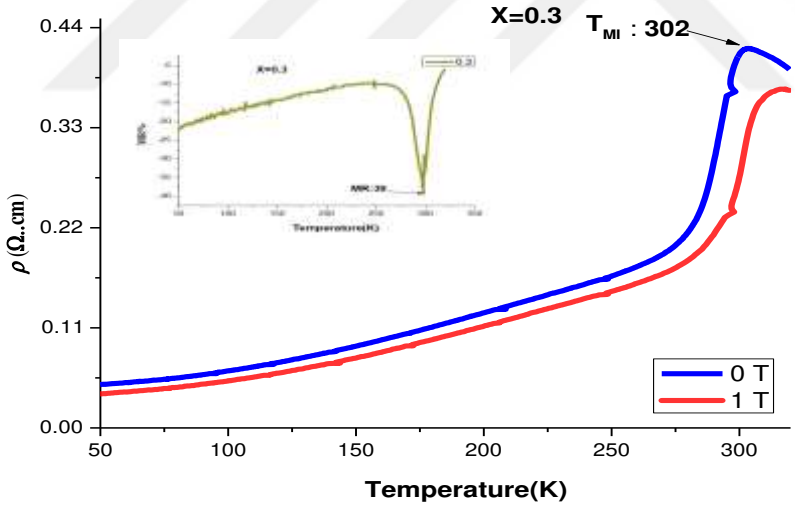

Fig 3.12 Resistivity dependence (ρ) on temperature graph for $Pr_{0.7}Sr_{03}MnO_3F_y$ sample under 0 and 1T magnetic fields. Included graph for MR % with temperature dependence on the same sample

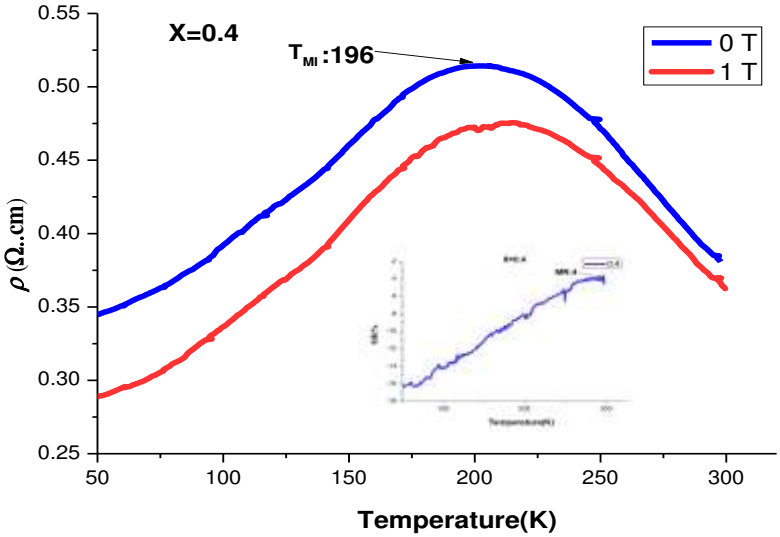

Fig 3.13 Resistivity dependence (ρ) on temperature graph for $Pr_{0.6}Sr_{0.4}MnO_3F_y$ sample under 0 and 1T magnetic fields. Included graph for MR % with temperature dependence on the same sample

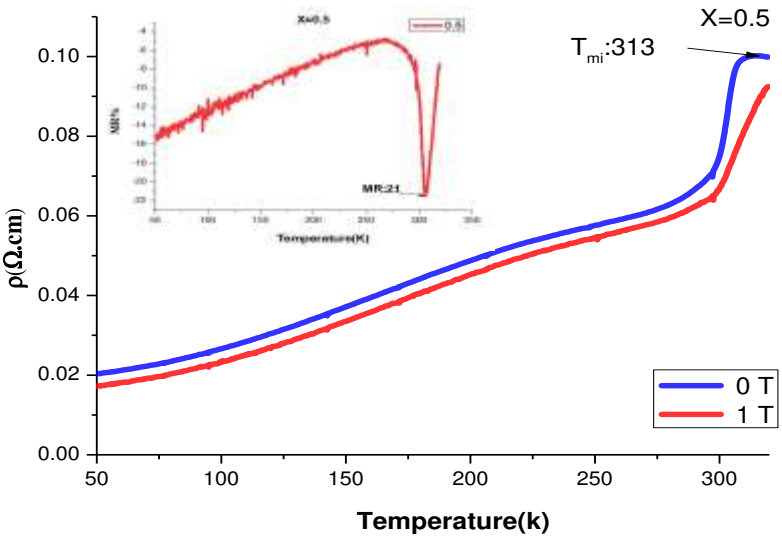

Fig 3.14 Resistivity dependence (ρ) on temperature graph for $Pr_{0.5}Sr_{0.5}MnO_3F_y$ sample under 0 and 1T magnetic fields. Included graph for MR % with temperature dependence on the same sample.

The sharpness of MI transition temperature is given by the temperature coefficient of resistance (TCR). The insets of the figures below show the TCR values for considered ceramic compounds. The TCR is quantified by the equation:

$$\%\,TCR\ = \frac{1}{\rho}\frac{d\rho}{dt} \times 100\,\%$$

where ρ and T are resistivity and temperature, respectively. For the *x=0.2* sample, the TCR % value is ~ 2 % K^{-1} and slightly decreases to ~ 4% K^{-1} with the *x=0.3* sample. As x rise to 0.5, we obtain the maximum TCR value (~5% K^{-1}) for the corresponding series. It is obvious that the Sr substitution at the A-site leads to an increment of the charge exchange in the networks of Mn – O. Therefore, the decrease in the system resistivity is obtained as mentioned above with lower polaron activation energy and higher TCR values. TCR value has a crucial role to enhance the sensitivity of uncooled infrared microbolometers.

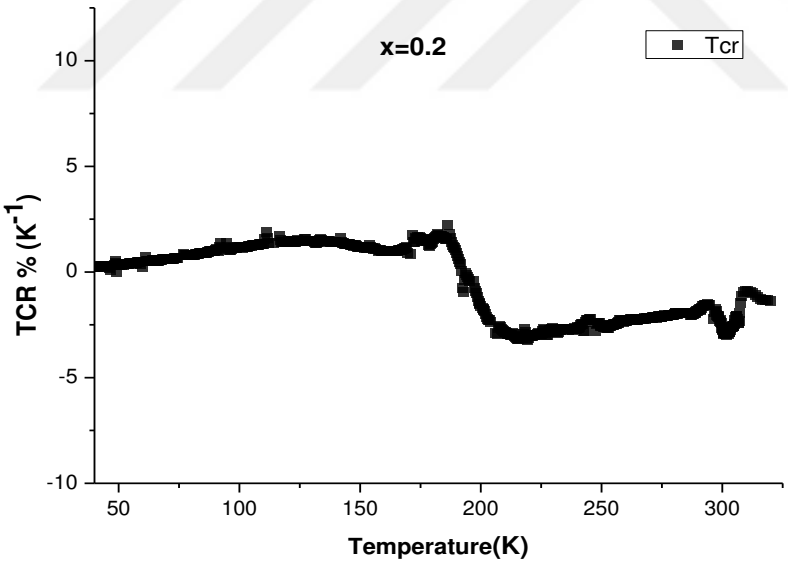

Fig 3.15. Temperature coefficient of resistance (TCR%) for $Pr_{0.8}Sr_{02}MnO_3F_y$

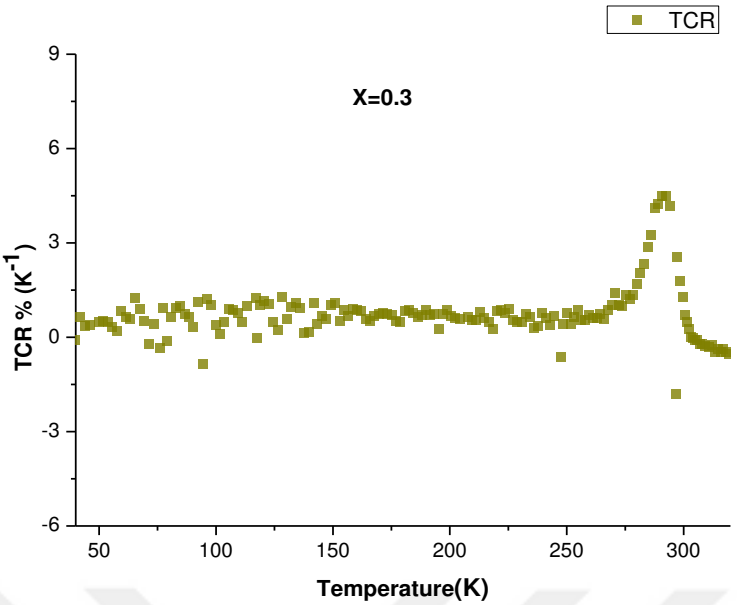

Fig 3.16. Temperature coefficient of resistance (TCR%) for $Pr_{0.7}Sr_{0.3}MnO_3F_y$

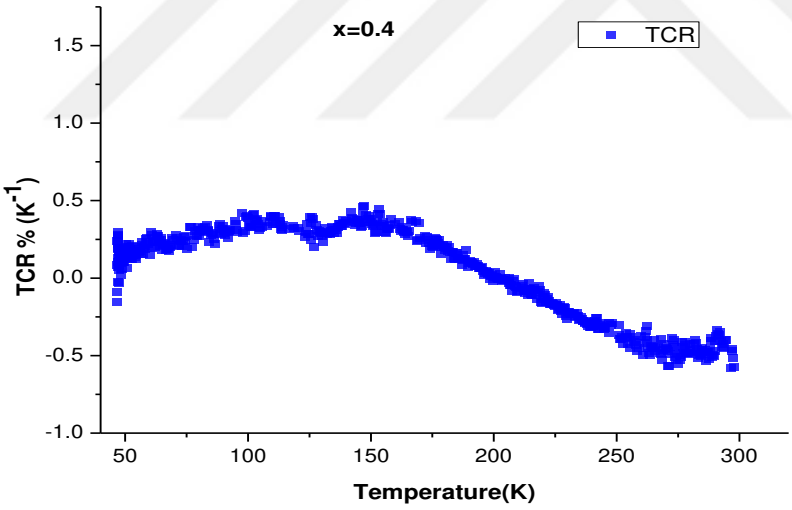

Fig 3.17. Temperature coefficient of resistance (TCR%) for $Pr_{0.6}Sr_{0.4}MnO_3F_y$

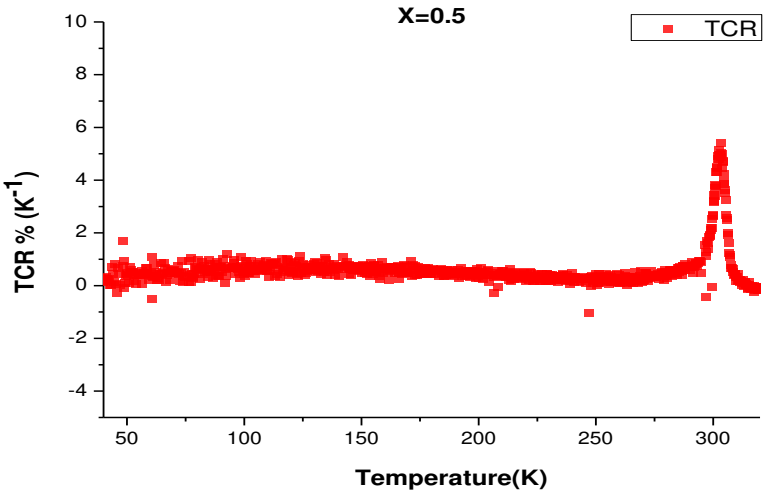

Fig 3.18. Temperature coefficient of resistance (TCR%) for $Pr_{0.5}Sr_{0.5}MnO_3F_y$

Table 3.3 The magnetic and electrical transport parameters for $Pr_{1-x}Sr_xMnO_3$ with x=(0.2, 0.3,0.4 and 0.5)

Compound	**T_{mi} (K)**	**MR_{max}%**	**MR_{max}% at T_{mi}**	**TCR_{max}%**	**TCR_{max}% at T_{mi}**
Pr0.8	191	35	190	2	186
Pr0.7	302	39	297	4	290
Pr0.6	196	4	298	0.4	147
Pr0.5	313	21	305	5	303

4. CONCLUSIONS AND RECOMMENDATIONS

All samples have an orthorhombic structure with Pnma space group N:62, according to X-ray diffraction. Besides, a second phase I41/AMD space group N:141 is observed in the samples $Pr_{0.5}Sr_{0.5}MnO_3F_y$.

The unit cell parameters decrease as doping concentration decreases. Except for the sample, x=0.5, this could be due to Sr^{+2}(1.45 Å) having a large ionic size compared to Pr^{+3}(1.29 Å).

The scanning electron microscope (SEM) analysis shows that all of the samples exhibit a granular morphology, with the average grain sizes decreasing as Sr concentration increases.

The (EDAX) analyses proved that all samples contain all expected elements (Pr, Sr, Mn, O), The analyses revealed what could be expected of these samples based on previous research.

Finally, when we analyze the electrical resistance from the inflection point (dp / dt) have noticed transition temperature T_{MI}, and metallic behavior obtained under the T_{MI} point.

In the region above the T_{MI}, semiconductor behaviors were observed, and the T_{MI} temperature increased, as did the ionic radius of (A-site) and the angle between Mn-O-Mn bonds.

It was observed that when an external magnetic field was applied, the percentage of MR values increased with decrease in the Pr content. It was noted that the examined TCR values for all samples took positive and negative values on the y-axis and were at the maximum value around T_{MI}.

5. REFERENCES

"Vancouver citation system was used in this thesis."

1- Tariq S, Mubarak AA, Kanwal B, Hamioud F, Afzal Q, Zahra S. Enlightening the stable ferromagnetic phase of SrAO3 (A= Cr, Fe and Co) compounds using spin polarized quantum mechanical approach. Chinese Journal of Physics. 2020 Feb 1;63:84-91.

2- Mokrane S, Bouafia H, Sahli B, Abidri B, Djebour B, Hiadsi S, Rached D. Pressure effect on mechanical, magnetic and optoelectronic properties of SrCoO3-Perovskite: FP-(L) APW+ lo investigation. Chinese Journal of Physics. 2019 Jun 1;59:625-40.

3- Arun B, Athira M, Akshay VR, Sudakshina B, Mutta GR, Vasundhara M. Investigation on the structural, magnetic and magnetocaloric properties of nanocrystalline Pr-deficient Pr1− xSrxMnO3− δ manganites. Journal of Magnetism and Magnetic Materials. 2018 Feb 15;448:322-31.

4- Thomson W. XIX. On the electro-dynamic qualities of metals:—Effects of magnetization on the electric conductivity of nickel and of iron. Proceedings of the Royal Society of London. 1857 Dec 31(8):546-50.

5- Millis AJ. Lattice effects in magnetoresistive manganese perovskites. Nature. 1998 Mar;392(6672):147-50.

6- Fontcuberta J. Colossal magnetoresistance. Physics World. 1999 Feb 1;12(2):33.

7- Maignan A, Raveau B, Martin C, Hervieu M. Large intragrain magnetoresistance above room temperature in the double perovskite Ba2FeMoO6. Journal of Solid State Chemistry. 1999 Apr 1;144(1):224-7.

8- Nkwachukwu OV, Arotiba OA. Perovskite Oxide–Based Materials for Photocatalytic and Photoelectrocatalytic Treatment of Water. Frontiers in Chemistry. 2021;9.

9- Xia W, Pei Z, Leng K, Zhu X. Research progress in rare earth-doped perovskite manganite oxide nanostructures. Nanoscale Research Letters. 2020 Dec;15(1):1-55.

10- Hazen RM. Perovskites. Scientific American. 1988 Jun 1;258(6):74-81.

11- Katz EA. Perovskite: name puzzle and German-Russian odyssey of discovery. Helvetica Chimica Acta. 2020 Jun;103(6):e2000061.

12- Megaw HD. Crystal structure of double oxides of the perovskite type. Proceedings of the Physical Society. 1946 Mar 1;58(2):133

13- Gispert JR. Coordination chemistry. Weinheim: Wiley-VCH; 2008 May 5.

14- Zhang W, Song Y. Multilayered Magnetic Thin Films for Electron Transport Control and Signal Sensing: From GMR, CMR, TMR to Quantum Anomalous Holzer Effect. Inorganic and Organic Thin Films: Fundamentals, Fabrication and Applications. 2021 May 3;1:95-123Maikhuri N, Gaur A, Aggarwal V, Gaur U, Singh HK. Magnetotransport Behaviour of Nanocrystalline Pr 1-x Sr x MnO 3 (0.40≤ x≤ 0.60). ISRN Materials Science. 2013 Jan 1

15- Prellier W, Singh MP, Murugavel P. The single-phase multiferroic oxides: from bulk to thin film. Journal of Physics: Condensed Matter. 2005 Jul 15;17(30):R803.

16- Martin LW, Crane SP, Chu YH, Holcomb MB, Gajek M, Huijben M, Yang CH, Balke N, Ramesh R. Multiferroics and magnetoelectrics: thin films and nanostructures. Journal of Physics: Condensed Matter. 2008 Oct 9;20(43):434220.

17- Sankarrajan S, Sakthipandi K, Rajendran V. Temperature-dependent sound velocities, attenuation and elastic moduli anomalies in Pr1− x Sr x MnO3 perovskite manganite materials at 0.28≤ X≤ 0.41. Phase Transitions. 2012 May 1;85(5):427-43.

18- Altintas SP, Mahamdioua N, Amira A, Terzioglu C. Effect of anionic substitution on the structural and magneto-electrical properties of La–Ca–Mn–O perovskite manganites. Journal of magnetism and magnetic materials. 2014 Nov 1;368:111-5.

19- Attfield JP, Kharlanov AL, McAllister JA. Cation effects in doped La2CuO4 superconductors. Nature. 1998 Jul;394(6689):157-9.

20- Elleuch F, Triki M, Bekri M, Dhahri E, Hlil EK. A-site-deficiency-dependent structural, magnetic and magnetoresistance properties in the Pr0. 6Sr0. 4MnO3 manganites. Journal of Alloys and Compounds. 2015 Jan 25;620:249-55.

21- Hwang HY, Cheong SW, Radaelli PG, Marezio M, Batlogg B. Lattice Effects on the Magnetoresistance in Doped LaMn O 3. Physical review letters. 1995 Jul 31;75(5):914.

22- Abdelmoula N, Guidara K, Cheikh–Rouhou A, Dhahri E, Joubert JC. Effects of the oxygen nonstoichiometry on the physical properties of La0. 7Sr0. 3MnO3− δ□ δ manganites (0≤ δ≤ 0.15). Journal of Solid State Chemistry. 2000 Apr 1;151(1):139-44.

23- Solanki PS, Doshi RR, Thaker CM, Pandya S, Ganesan V, Kuberkar DG. Transport and magnetotransport studies on sol–gel grown nanostructured La0. 7Pb0. 3MnO3 manganites. Journal of Nanoscience and Nanotechnology. 2009 Sep 1;9(9):5681-6.
24- Parmar RN, Markna JH, Solanki PS, Doshi RR, Vachhani PS, Kuberkar DG. Grain Size Dependent Transport and Magnetoresistance Behavior of Chemical Solution Deposition Grown Nanostructured La0 7Sr0 3MnO3 Manganite Films. Journal of Nanoscience and Nanotechnology. 2008 Aug 1;8(8):4146-51.
25- Mather ND. G. Burnell, SP Issac, TFJ ackson, B. S. Teo,.. L. McManus-Driscoll, L. F. Cohen, JE Evetts, MG Blamire, Nature. 1997;387:266.
26- Shaikh MW, Varshney D. Structural and electrical properties of $Pr_{1-x}Sr_xMnO_3$ (x= 0.25, 0.3, 0.35 and 0.4) manganites. Materials science in semiconductor processing. 2014 Nov 1;27:418-26.